LBL-25260 c.2

Center for Advanced Materials

CAM

RECEIVED
LAWRENCE
BERKELEY LABORATORY

JUN 23 1988

LIBRARY AND
DOCUMENTS SECTION

Theoretical Predictions of Precipitate Shapes in Cubic Alloys

T.S. Edgecumbe
(M.S. Thesis)

May 1988

TWO-WEEK LOAN COPY

This is a Library Circulating Copy which may be borrowed for two weeks.

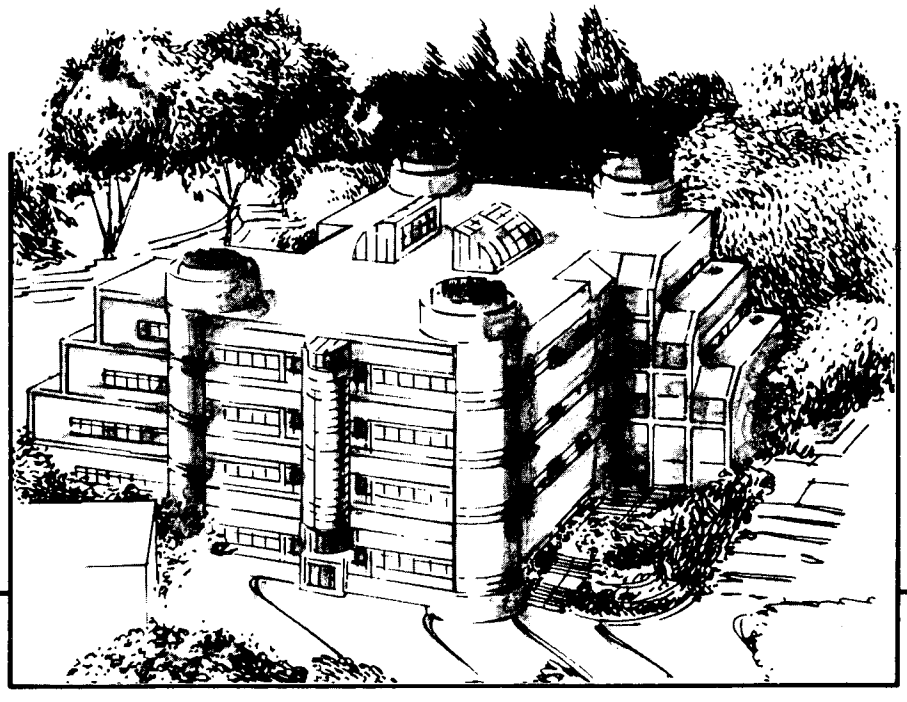

Materials and Chemical Sciences Division

Lawrence Berkeley Laboratory • University of California

ONE CYCLOTRON ROAD, BERKELEY, CA 94720 • (415) 486-4755

Prepared for the U.S. Department of Energy under Contract DE-AC03-76SF00098

LBL-25260 c.2

DISCLAIMER

This document was prepared as an account of work sponsored by the United States Government. While this document is believed to contain correct information, neither the United States Government nor any agency thereof, nor the Regents of the University of California, nor any of their employees, makes any warranty, express or implied, or assumes any legal responsibility for the accuracy, completeness, or usefulness of any information, apparatus, product, or process disclosed, or represents that its use would not infringe privately owned rights. Reference herein to any specific commercial product, process, or service by its trade name, trademark, manufacturer, or otherwise, does not necessarily constitute or imply its endorsement, recommendation, or favoring by the United States Government or any agency thereof, or the Regents of the University of California. The views and opinions of authors expressed herein do not necessarily state or reflect those of the United States Government or any agency thereof or the Regents of the University of California.

LBL 25260

Theoretical Predictions of Precipitate Shapes in Cubic Alloys

Tammy Suzanne Edgecumbe

M. S. Thesis

Department of Materials Science and Mineral Engineering
University of California at Berkeley
Berkeley, California 94720
and
Center for Advanced Materials
Materials and Chemical Sciences Division
Lawrence Berkeley Laboratory
University of California

May 1988

This work is jointly supported by the Director, Office of Energy Research,
Office of Basic Energy Science, Materials Sciences Division of the
U. S. Department of Energy under Control No. DE-AC03-76SF00098

Abstract

The equilibrium shape of an isolated, coherent precipitate in an elastic solid is determined by the minimum in the free energy which is the sum of the elastic and surface energies. The elastic free energy, which is minimized when the precipitate takes on the form of a thin plate, was calculated using the Khachaturyan formulation. The surface energy which was assumed to be isotropic is minimized when the precipitate is spherical. These two contributions were found to sum in such a way that the precipitate is spherical at small volumes, cuboidal at intermediate volumes, and eventually spreads into a plate of increasing aspect ratio beyond a certain critical volume. The volume at which these shape transitions occur depends on the surface tension, the volume change on forming the inclusion (i.e. the misfit), and the elastic constants. These critical volumes were calculated and compared to those volumes seen experimentally for the Ni-Al, Ni-Ti and Al-Li binary systems which form the cubic Ni_3Al (γ'), Ni_3Ti (γ') and Al_3Li (δ') precipitates, respectively.

Good quantitative agreement between theory and experiment was obtained for the sphere to cube transition in the three systems investigated. For typical Ni-Al and Ni-Ti alloys, the γ' sphere to cube shape transition is expected to occur at about 110 Å and 130 Å, respectively. Spherical δ' precipitates were found to be stable until rather large volumes (30 μm^3) for the most part due to the low δ'-Al misfit. The stability of spherical δ' precipitates is also likely due to the relative isotropy of Al.

Plate-like precipitates in the Ni-base alloys were found to be

stable at volumes in excess of $(130)^3$-$(200Å)^3$. The cube to plate shape transition of an isolated precipitate will occur at the volume predicted if the cuboidal shape is unstable with respect to the plate beyond the critical volume. If the cuboidal shape is metastable, however, the shape transition may not occur until much larger volumes. A plate-shaped precipitate may also be formed by the coalescence of an array of interacting cubes. The transition volumes in this case are most likely greater than the values predicted for the isolated inclusion for two reasons. First an array of interacting cubes must have a lower free energy per unit volume than a single isolated cube making it stable to larger volumes than the single cube. Second, an array of cubes will not coalesce to form a plate if the aspect ratio and volume of the plate is such that the free energy increases.

ACKNOWLEDGEMENT

My deepest appreciation goes to my advisor, Professor J.W. Morris, Jr., without whose help this project could not have been completed. The contribution of Professor A.G. Khachaturyan is obvious and also appreciated. My committee members: Professors Morris, Khachaturyan and Thomas deserve a special thanks for taking the time to read my thesis both thoroughly and quickly and for their useful comments and suggestions.

I also must mention Judy Glazer and Doug Marinaro whose many discussions concerning the experimental and computer aspects of my thesis work were invaluable.

Finally, I would like to express my appreciation to my husband, Lenny Summers, who helped both directly and indirectly in the completion of this project.

THEORETICAL PREDICTIONS OF PRECIPITATE SHAPES IN CUBIC ALLOYS

TABLE OF CONTENTS

Section 1. Introduction 1

1.1. The Preferred Shape from Strengthening Considerations 1

1.2. Examples of Alloys Hardened by Cubic Precipitates. .2

1.3. The Shapes Observed for γ' and δ' Precipitates 4

1.4. Modeling the Observed Precipitate Shapes 5

1.5. Alloys Used for Calculations 5

Section 2. The Elastic Free Energy. 7

2.1. The Macroscopic Theory 7

2.2. Examples 17

2.2.1. The Elastically Preferred Shape. 17

2.2.2. Ellipsoidal Precipitates 19

2.2.2.1. Elastic Theory 19

2.2.2.2. Approach to Computer Calculations 21

2.2.3. Cuboidal Precipitates. 24

Section 3. The Surface Energy 28

3.1. The Surface Energy of an Ellipsoidal Precipitate . 28

3.2. The Surface Energy of a Cuboidal Precipitate . . . 29

Section 4. The Preferred Shape. 31

Section 5. Numerical Results. 33

Section 6. Discussion 37

6.1. The Sphere to Cube Transition. 37

6.2. The Cube to Plate Transition 38

6.3. The Effect of Anisotropy and Misfit on the Critical Particle Sizes. 41

6.4. The Validity of the Homogeneous Elastic Constants Assumption 42

Section 7. Conclusions. 45

References 47

Tables 50

Figures. 54

Appendix 1: The Symmetry of the Taylor Expansion Coefficients α_{ij} and λ_{ijkl} 62

Appendix 2: Gauss' Theorem. 63

Appendix 3: The Fourier Transform of the Derivative of a Function . 64

Appendix 4: The Convolution Theorem 65

Appendix 5: The Shape of a Tetragonal Precipitate in a Cubic Alloy. 66

1. Introduction

1.1. The Preferred Precipitate Shape from Strengthening Considerations

The shape of a coherent precipitate can have a large effect on its ability to pin dislocations and therefore on the strength of the alloy that forms it. The free energy terms which must be taken into account in determining the shape of a precipitate are the elastic and surface energies. As the matrix-precipitate misfit increases, the elastic free energy contributes more and more to the total free energy. Eventually, beyond a certain misfit, the elastic free energy is dominant and virtually determines the precipitate shape. As will be shown in a subsequent section, the precipitate shape which minimizes the elastic free energy is a plate. Hence, plate-shaped precipitates tend to form in high-misfit alloys. Since misfit strengthening is a potent form of precipitation hardening, plate-shaped precipitates are often associated with the stronger precipitation-hardened alloys.

There are, on the other hand, a couple of reasons why a coherent plate-shaped precipitate provides the most strengthening for a given alloy system. The first of these is due to the distribution of the strain in and around the precipitate. From elastic theory, it has been found that a large part of the misfit strain caused by the difference between the plate-shaped precipitate and matrix lattices is concentrated in a direction along the precipitate habit plane normal [1]. Since the precipitate and matrix crystal structures provide only a finite amount of strain, this concentration of the strain provides, in most directions, a much more effective dislocation barrier than if

the strain were evenly distributed in all directions. If the precipitate had only one habit plane, however, the strength of the alloy would be directional. Fortunately, cubic alloys are almost invariably used so the precipitate plates generally have more than one habit plane related to each other by cubic symmetry operations. For this reason the concentration of the misfit strain does not usually lead to directional properties.

As discussed by Glazer [2], a second reason for the effective strengthening of plate-shaped precipitates is geometrical in nature. For precipitates which are ordered with little or no misfit with the matrix, the effectiveness of a precipitate at pinning dislocations depends on the maximum instantaneous force required to push the dislocation by an infinitesimal amount through the precipitate. This force in turn depends only on the maximum width of the precipitate parallel to the dislocation in its glide plane, not on the precipitate thickness. A plate-shaped precipitate, then, not only provides more obstacles by crossing more glide planes, but it provides stronger obstacles because it is potentially wider in the dislocation glide plane than a more equiaxed precipitate such as a sphere of the same volume. In other words, the plate shape does not "waste" as much of its volume on thickness as does a sphere.

1.2. Examples of Alloys Hardened by Cubic Precipitates

The best combination of strength and toughness in precipitation-hardened alloys is generally obtained with coherent precipitates because they tend to form in a uniform distribution throughout the bulk

of the alloy. Because coherent precipitates are usually a transition phase between the solid solution and the equilibrium phases, they quite often have the same crystal symmetry as the parent solid solution phase. As a result, many of the coherent precipitates encountered in practice are cubic since most of the alloys used in engineering applications are. For this reason, emphasis in this work was placed on the shape of cubic precipitates in cubic alloys.

Probably the most thoroughly investigated group of alloys hardened by cubic precipitates are the superalloys. Superalloys are said to be Fe or Ni based depending on which element is the major component. Elements such as Ti and Al are added so the precipitate ($Ni_3(Al,Ti)$) will form. Large elements such as Nb and Ta which partition to the precipitate are added to increase the lattice mismatch with the matrix. V, B, and Mo are often added to improve grain boundary properties. Oxidation resistance is usually achieved through Cr additions, and several other elements may be added for various reasons such as W for solid-solution hardening. In addition, Ni is usually added to Fe-based superalloys not only for the precipitation reaction but also to stabilize the fcc austenite phase. Sullivan and Donachie [3] and Decker [4] give a good review of the Fe- and Ni-base superalloys, respectively.

Al-Li alloys have also been studied extensively and, because of the low weight of Li, are generating much interest in the aerospace industry. Not many elements are added to these alloys in order to keep the density low. Li and Cu are added to form the Al_3Li, Al_2CuLi and Al_2Cu precipitates. Sometimes elements such as Mg are added as solid solution strengtheners. See Narayanan et al. [5] for a good review of

the low-density Al alloys.

The completely coherent, cubic precipitates which form in these alloys are γ' ($Ni_3(Al,Ti)$) and δ' (Al_3Li). The $Ni_3(Al,Ti)$ precipitate is called γ' whether it is present in Ni- or Fe-base alloys. Its composition can be Ni_3Al or Ni_3Ti or anywhere in between including fourth or more element additions. Very few elements have been found to segregate to δ' so δ' generally refers to the Al_3Li phase. Both γ' and δ' are cubic with the fcc-based, ordered $L1_2$ crystal structure shown in Figure 1.

1.3. The Shapes Observed for γ' and δ' Precipitates

In the continuum limit, precipitates of δ' take on a spherical shape at all volumes observed. Precipitates of γ', on the other hand, have been reported to take on several shapes. When very small, γ' precipitates are spherical. Early on in coarsening, however, they change shape by flattening on the six {100} faces to become cubes. Later during coarsening, these cubes tend to line up along ⟨100⟩ directions until, in some instances, they appear to coalesce and form plates [6,7]. By predicting precipitate shape as a function of its volume in a given alloy, this work was undertaken to determine whether these plate-shaped precipitates should be expected to form and what, if anything, can be done to increase the probability of their forming.

1.4 Modeling the Observed Precipitate Shapes

To describe the spherical and plate shapes, an ellipsoid of revolution about the [001] axis was used. Thus, by varying the aspect ratio, K (defined as the semi-axis in the habit plane divided by the unique semi-axis along the habit plane normal), this model can continuously describe shapes from a rod (semi-major axis perpendicular to the (001) habit plane, $K<1$) to a sphere ($K=1$) to a plate (semi-major axis parallel to the (001) habit plane, $K>1$). The cuboidal precipitates were modeled as cubes.

The preferred shape of an isolated precipitate is determined by minimizing the sum of the surface and elastic free energies. Khachaturyan's formulation [1,8] was used to calculate the elastic free energy, and an isotropic surface energy was assumed.

1.5 Alloys Used for Calculations

For the purpose of comparison to the theoretical results of this investigation, only binary alloys were used. Because the Ni-Al, Ni-Ti, and Al-Li alloys have been thoroughly studied, they were chosen. The γ' phase which forms in the Ni-Al alloys is an equilibrium phase, but γ' (Ni_3Ti) is only metastable in the Ni-Ti alloys. The incoherent η phase, which is hexagonal and also has the stoichiometric composition Ni_3Ti, is the equilibrium second phase in Ni-Ti alloys. Likewise, the δ' phase is only metastable in Al-Li alloys. The equilibrium second phase in Al-Li alloys is δ (AlLi) which has the bcc-based, ordered NaTl structure.

The Fe-based superalloys were not represented in this work mainly because it would have been impossible with a binary alloy. At least three elements are required: Fe, Ni to stabilize the austenite phase as well as to precipitate γ', and Al or Ti to precipitate γ'; but most of the experimental work has been done on much more complicated alloys. This makes comparison of theoretical results to experimental observations difficult because parameters such as the misfit strain vary considerably with composition. Also, because of the relatively large number of elements in Fe-based superalloys, there are a large number of equilibrium phases which form at the expense of the metastable γ' precipitates. For this reason, γ' precipitates don't tend to coarsen to very large sizes in practice which is a disadvantage when trying to compare the shape of the precipitate as a function of its volume to theoretical results.

2. The Elastic Free Energy

In the late 1950's, Eshelby [9-11] formulated an expression for the strain energy of a precipitate with an ellipsoidal shape in an isotropic medium assuming the elastic constants of the precipitate and the matrix were similar. Since then, many authors have extended and utilized this approach [12-17]. In 1967, Khachaturyan [8], who also assumed that the elastic constants were homogeneous, extended this theory to a precipitate of arbitrary shape in an elastically anisotropic medium using a Fourier transform technique. These results have been used extensively as well [1,18-24]. This latter theory is used here.

Khachaturyan's expression for the elastic free energy may be derived from a continuum (macroscopic) or a discrete lattice (microscopic) point of view. The two approaches lead to expressions that are equivalent. Since the macroscopic theory is more applicable to the case of large defects such as precipitates, only it will be discussed in the following. Detailed discussions of the microscopic theory may be found elsewhere [1,18,19].

2.1 The Macroscopic Theory

The elastic free energy is a function of the displacement field $\mathbf{u}(\mathbf{r}')$. By expanding $\mathbf{u}(\mathbf{r}')$ to first order about the point $\mathbf{r}$, the incremental elastic free energy per unit volume may be written in the form

$$f(\mathbf{r}) = \tilde{f}[u_i(\mathbf{r}), u_{i,j}(\mathbf{r})] \tag{2.1.1}$$

where an index preceded by a comma denotes differentiation with respect to the cartesian coordinates, $u_{i,j}(\mathbf{r}) = \partial u_i(\mathbf{r})/\partial r_j$. Since the free energy must be invariant to rigid-body translations, it cannot depend on $\mathbf{u}(\mathbf{r})$. It then follows that the elastic free energy is expressible in the form

$$F_{el} = \int \tilde{f}[u_{i,j}(\mathbf{r})]d^3r \tag{2.1.2}$$

where the integral is taken over the entire system.

If the displacement gradients are broken up into the symmetric and antisymmetric tensors:

$$\varepsilon_{ij}(\mathbf{r})=(1/2)[u_{i,j}(\mathbf{r}) + u_{j,i}(\mathbf{r})]$$

and (2.1.3)

$$\omega_{ij}(\mathbf{r})=(1/2)[u_{i,j}(\mathbf{r}) - u_{j,i}(\mathbf{r})]$$

such that $u_{i,j}(\mathbf{r})=\varepsilon_{ij}(\mathbf{r})+\omega_{ij}(\mathbf{r})$ where $\varepsilon_{ij}(\mathbf{r})$ is the infinitesimal strain tensor and $\omega_{ij}(\mathbf{r})$ is the rotation tensor, then equation (2.1.2) may be written as

$$F_{el} = \int \tilde{f}[\varepsilon_{ij}(\mathbf{r}), \omega_{ij}(\mathbf{r})]d^3r. \tag{2.1.4}$$

The free energy, however, must be invariant to rigid-body rotations. It therefore cannot depend on $\omega_{ij}(\mathbf{r})$ since it is always possible for

$\omega_{ij}(\mathbf{r})$ to take on a value which is constant throughout the system (i.e. a rigid-body rotation). Equation (2.1.4) can then be written in the following simplified form:

$$F_{el} = \int \tilde{f}[\varepsilon_{ij}(\mathbf{r})]d^3r. \tag{2.1.5}$$

If the reference state is defined as undistorted material ($\varepsilon_{ij}=0$) and if $\tilde{f}[\varepsilon_{ij}(\mathbf{r})]$ is continuous in $\varepsilon_{ij}(\mathbf{r})$ (requiring second phases to be coherent), then a second-order expansion of $\tilde{f}[\varepsilon_{ij}(\mathbf{r})]$ about the reference state yields

$$\tilde{f}[\varepsilon_{ij}(\mathbf{r})] = \alpha_{ij}\varepsilon_{ij}(\mathbf{r}) + (1/2)\lambda_{ijkl}\varepsilon_{ij}(\mathbf{r})\varepsilon_{kl}(\mathbf{r}) \tag{2.1.6}$$

where α_{ij} and λ_{ijkl} are the first- and second-order expansion coefficients, respectively, and the terms are to be summed over the indices from 1 to 3 if the indices are repeated.

Two points can be made from these results. First, as shown in Appendix 1, requiring that the free energy be invariant to rigid-body rotations, requires that the tensor, α_{ij} be symmetric:

$$\alpha_{ij}=\alpha_{ji}$$

and that (2.1.7)

$$\lambda_{ijkl} = \lambda_{ijlk} = \lambda_{jikl} = \lambda_{klij}.$$

Second, the stress tensor is defined by

$$\sigma_{ij}(\mathbf{r}) = \partial f[\varepsilon_{ij}(\mathbf{r})]/\partial\varepsilon_{ij}(\mathbf{r}) = \alpha_{ij} + \lambda_{ijkl}\varepsilon_{kl}(\mathbf{r}). \tag{2.1.8}$$

This is just Hooke's law with λ_{ijkl} being the elastic stiffness tensor for the material.

As originally suggested by Eshelby [9], the elastic free energy changes associated with a precipitation reaction can be found by considering the transformation as taking place in the five steps shown schematically in Figure 2. The region which is to transform is cut and removed from the matrix. The free energy change associated with the creation of new surface is partially compensated for in step 4. Any remaining surface effects will be considered separately in a later section. The elastic energy change associated with this first step is zero.

The material which has been removed is then allowed to transform under stress-free conditions. Because there is no stress, the free energy change associated with the second step is zero. The strain at this point is nonzero, however, and is usually called the stress-free transformation strain, ε^o. It is defined in terms of the lattice parameters of the matrix and the unconstrained precipitate lattice parameters.

So that the precipitate may be reinserted in the matrix without strain, a traction is applied to its surface until the strain is zero with respect to the reference state. Since this is simply a shape reversal, the strain for the third step is $-\varepsilon^o$. The free energy change associated with this step is then:

$$F^3_{el} = (1/2)\lambda^{(ppt)}_{ijkl}\varepsilon^o_{ij}\varepsilon^o_{kl}V \qquad (2.1.9)$$

where $\lambda_{ijkl}^{(ppt)}$ is the precipitate elastic stiffness tensor and V is its volume. This energy is often called the self energy.

Once the particle is placed back in the matrix and 'welded' in, the tractions are removed allowing the precipitate to relax. From equations (2.1.5) and (2.1.6), the elastic free energy associated with this relaxation may be expressed as

$$F_{el}^{5,ppt} = \int_{ppt}[\alpha_{ij}\varepsilon_{ij}(r) + (1/2)\lambda_{ijkl}^{(ppt)}\varepsilon_{ij}(r)\varepsilon_{kl}(r)]d^3r \quad (2.1.10)$$

within the precipitate and

$$F_{el}^{5,matrix} = \int_{matrix} (1/2)\lambda_{ijkl}^{(matrix)}\varepsilon_{ij}(r)\varepsilon_{kl}(r)d^3r \quad (2.1.11)$$

within the matrix where $\lambda_{ijkl}^{(matrix)}$ is the matrix elastic stiffness tensor. By equation (2.1.8), $\alpha_{ij} = 0$ within the matrix since the stress in the matrix is zero when the strain is zero.

Within the precipitate when the strain is zero, the stress is given by

$$\sigma_{ij}^{(ppt)}(r)|_{\varepsilon=0} = -\lambda_{ijkl}^{(ppt)}\varepsilon_{kl}^{o} = -\sigma_{ij}^{o} \quad (2.1.12)$$

where σ_{ij}^{o} is often called the transformation stress. Plugging (2.1.12) into equation (2.1.8) for $\varepsilon_{kl}(r)=0$ yields

$$\alpha_{ij} = -\lambda_{ijkl}^{(ppt)}\varepsilon_{kl}^{o} = -\sigma_{ij}^{o}. \quad (2.1.13)$$

Combining (2.1.9) and (2.1.10) and substituting equation (2.1.13) for

α_{ij} then gives for the elastic free energy within the inclusion

$$F_{el}^{ppt} = (1/2)\lambda_{ijkl}^{(ppt)}\varepsilon_{ij}^{o}\varepsilon_{kl}^{o}V + \int_{ppt} [-\sigma_{ij}^{o}\varepsilon_{ij}(r) + (1/2)\lambda_{ijkl}^{(ppt)}\varepsilon_{ij}(r)\varepsilon_{kl}(r)]\, d^3r. \tag{2.1.14}$$

The mathematics become formidable when equations (2.1.11) and (2.1.14) are combined. A common approximation which makes the mathematics easier to handle is that of homogeneous elastic constants (i.e. the precipitate and matrix elastic constants are the same). This assumption will be made here; its validity will be discussed in a later section. Combination of equations (2.1.11) and (2.1.14) now gives

$$F_{el} = F_{el}^{o} + \int [-\sigma_{ij}^{o}\theta(r)\varepsilon_{ij}(r) + (1/2)\lambda_{ijkl}\varepsilon_{ij}(r)\varepsilon_{kl}(r)]\, d^3r. \tag{2.1.15}$$

where the integral is taken over the entire system, $F_{el}^{o} = (1/2)\lambda_{ijkl}\varepsilon_{ij}^{o}\varepsilon_{kl}^{o}V$ is the self energy, and $\theta(r)$ is the shape factor defined as

$$\theta(r) = \begin{cases} 1 & r \text{ inside the precipitate} \\ 0 & \text{otherwise.} \end{cases} \tag{2.1.16}$$

Equilibrium requires that the free energy be a minimum with respect to arbitrary infinitesimal fluctuations in the state of the system at constant temperature. This condition, in mathematical terms, says that $\delta F = 0$. From equation (2.1.15) then

$$\delta F_{el} = \int [\ -\sigma^o_{ij}\theta(\mathbf{r})\delta\varepsilon_{ij}(\mathbf{r})$$

$$+ (1/2)\lambda_{ijkl}\delta(\varepsilon_{ij}(\mathbf{r}))\varepsilon_{kl}(\mathbf{r}) \qquad (2.1.17)$$

$$+ (1/2)\lambda_{ijkl}\varepsilon_{ij}(\mathbf{r})\delta(\varepsilon_{kl}(\mathbf{r}))]\ d^3r = 0.$$

Using the definition of the infinitesimal strain in equation (2.1.3), equation (2.1.17) can be written in terms of the displacements:

$$\delta F_{el} = \int [-\sigma^o_{ij}\theta(\mathbf{r})[\delta u_i(\mathbf{r})]_{,j} + \lambda_{ijkl}[\delta u_i(\mathbf{r})]_{,j}\varepsilon_{kl}(\mathbf{r})]\ d^3r = 0 \qquad (2.1.18)$$

where the symmetry of σ^o_{ij} and λ_{ijkl} (equations (2.1.7) and (2.1.13)) has been used to simplify the expression. Using the product rule of differentiation,

$$\delta F_{el} = \int [\sigma^o_{ij}\theta_{,j}(\mathbf{r})\delta u_i(\mathbf{r}) - \lambda_{ijkl}\varepsilon_{kl,j}(\mathbf{r})\delta u_i(\mathbf{r})]\ d^3r$$

$$+\int [-\sigma^o_{ij}\theta(\mathbf{r})\delta u_i(\mathbf{r}) + \lambda_{ijkl}\delta u_i(\mathbf{r})\varepsilon_{kl}(\mathbf{r})]_{,j}\ d^3r \qquad (2.1.19)$$

$$= 0.$$

Using Gauss' theorem and the fact that the stress vanishes at the surface, it can be shown that the second term in equation (2.1.19) is zero (see Appendix 2). Equation (2.1.19) then simplifies to

$$\delta F = \int [\sigma^o_{ij}\theta_{,j}(\mathbf{r}) - \lambda_{ijkl}\varepsilon_{kl,j}(\mathbf{r})]\delta u_i(\mathbf{r})\ d^3r = 0. \qquad (2.1.20)$$

Equation (2.1.20) holds for arbitrary displacements $\delta u_i(\mathbf{r})$ if and only if

$$\sigma^o_{ij}\theta_{,j}(\mathbf{r}) = \lambda_{ijkl}\varepsilon_{kl,j}(\mathbf{r}) = \lambda_{ijkl}u_{l,jk}(\mathbf{r}). \tag{2.1.21}$$

Using the method illustrated in Appendix 3, it can be shown that the Fourier transform of equation (2.1.21) is

$$i\sigma^o_{ij}k_j\theta(\mathbf{k}) = -\lambda_{ijkl}k_jk_ku_l(\mathbf{k}) = -G^{-1}_{il}(\mathbf{k})u_l(\mathbf{k}) \tag{2.1.22}$$

where $G^{-1}_{il}(\mathbf{k})=\lambda_{ijkl}k_jk_k$ is the dynamical matrix tensor in the long-wavelength limit. Solving equation (2.1.22) for the displacements gives

$$u_l(\mathbf{k}) = -ik_j\sigma^o_{ji}G_{il}(\mathbf{k})\theta(\mathbf{k}). \tag{2.1.23}$$

Using the convolution theorem, equation (2.1.15) for the elastic free energy can be rewritten (see Appendix 4):

$$F_{el} = F^o_{el} + \int [-\sigma^o_{ij}\theta(\mathbf{k})\varepsilon^*_{ij}(\mathbf{k}) + (1/2)\lambda_{ijkl}\varepsilon_{ij}(\mathbf{k})\varepsilon^*_{kl}(\mathbf{k})]d^3k/(2\pi)^3. \tag{2.1.24}$$

The Fourier transform of the equation for the infinitesimal strain in equation (2.1.3) is

$$\varepsilon_{ij}(\mathbf{k}) = (i/2)[k_j u_i(\mathbf{k}) + k_i u_j(\mathbf{k})]. \tag{2.1.25}$$

Because the transformation stress is symmetric, the product of the transformation stress and the complex conjugate of the strain may be written as

$$\sigma^o_{ij}\varepsilon^*_{ij}(\mathbf{k}) = -i\sigma^o{}_{ij}k_i u^*_j(\mathbf{k}). \tag{2.1.26}$$

Also, since $\lambda_{ijkl}=\lambda_{jikl}=\lambda_{ijlk}$, the product of the elastic stiffness tensor and the square of the infinitesimal strain is given by

$$\lambda_{ijkl}\varepsilon_{ij}(\mathbf{k})\varepsilon^*_{kl}(\mathbf{k}) = \lambda_{ijkl}k_i u_j(\mathbf{k})k_k u^*_l(\mathbf{k}). \tag{2.1.27}$$

Equation (2.1.24) may then be simplified to give

$$\begin{aligned} F_{el} = F^o_{el} + \int [&i\sigma^o_{ij}k_i u^*_j(\mathbf{k})\theta(\mathbf{k}) \\ &+ (1/2)\lambda_{ijkl}k_i k_k u_j(\mathbf{k})u^*_l(\mathbf{k})]d^3k/(2\pi)^3. \end{aligned} \tag{2.1.28}$$

Substitution of equation (2.1.23) into equation (2.1.28) yields

$$F_{el} = F^o_{el} - (1/2)\int [k_i\sigma^o_{ij}G_{jk}(\mathbf{k})\sigma^o_{kl}k_l]|\theta(\mathbf{k})|^2 d^3k/(2\pi)^3 \tag{2.1.29}$$

where the definition of $G_{ij}^{-1}(\mathbf{k})$ and the symmetry of $G_{ij}(\mathbf{k})$, σ_{ij}^{o} and λ_{ijkl} have been used.

Let

$$\Omega_{ij}^{-1}(\mathbf{n}) = G_{ij}^{-1}(\mathbf{k})/|\mathbf{k}|^2 = \lambda_{iklj}n_k n_l \tag{2.1.30}$$

where $\mathbf{n} = \mathbf{k}/|\mathbf{k}|$ is a unit vector in the $\mathbf{k}$ direction. Then

$$\Omega_{ij}(\mathbf{n}) = |\mathbf{k}|^2 G_{ij}(\mathbf{k}), \tag{2.1.31}$$

and equation (2.1.29) may be rewritten as

$$F_{el} = F_{el}^{o} - (1/2)\int [n_i\sigma_{ij}^{o}\Omega_{jk}(\mathbf{n})\sigma_{kl}^{o}n_l]|\Theta(\mathbf{k})|^2 d^3k/(2\pi)^3. \tag{2.1.32}$$

Since by definition

$$\int |\Theta(\mathbf{k})|^2 d^3k/(2\pi)^3 = V, \tag{2.1.33}$$

equation (2.1.32) may be written in the following more compact form.

$$F_{el} = (1/2)\int B(\mathbf{n})|\Theta(\mathbf{k})|^2 \, d^3k/(2\pi)^3 \tag{2.1.34}$$

where $B(\mathbf{n}) = \lambda_{ijkl}\varepsilon_{ij}^{o}\varepsilon_{kl}^{o} - n_i\sigma_{ij}^{o}\Omega_{jk}(\mathbf{n})\sigma_{kl}^{o}n_l$. $B(\mathbf{n})$ depends on the material properties (i.e. the elastic constants and the crystal structures). $\Theta(\mathbf{k})$ depends only on the shape of the precipitate and not on the materials involved.

2.2. Examples

2.2.1. The Elastically Preferred Shape

In the limit of large particle sizes where the surface to volume ratio is small, the surface energy is negligible. When this is the case, minimization of the strain energy, equation (2.1.34), determines the preferred shape of the precipitate.

If $B(\mathbf{n})$ is a continuous function of $\mathbf{n}$, then by the mean value theorem,

$$\begin{aligned} F_{el} &\geqslant (1/2)\min[B(\mathbf{n})]\int|\Theta(\mathbf{k})|^2 d^3k/(2\pi)^3 \\ &\geqslant (V/2)\min[B(\mathbf{n})] \end{aligned} \tag{2.2.1}$$

where equation (2.1.33) has been used to obtain the second form of the above equation. If $\mathbf{n}=\mathbf{n}^o$ is the vector which minimizes $B(\mathbf{n})$, then equation (2.2.1) may be rewritten as

$$F_{el} \geqslant (V/2)B(\mathbf{n}^o) \tag{2.2.2}$$

where $B(\mathbf{n}^o) = \lambda_{ijkl}\sigma^o_{ij}\varepsilon^o_{kl} - n^o_i\sigma^o_{ij}\Omega_{jk}\sigma^o_{kl}n^o_l$. Equation (2.2.2) becomes an equality when $B(\mathbf{n}) = B(\mathbf{n}^o)$ for all values of $\mathbf{n}$ for which $\Theta(\mathbf{k})$ is nonzero.

Consider first the case where there is only one value of $\mathbf{n}^o$ for which $B(\mathbf{n})$ is a minimum. This restriction requires that $\Theta(\mathbf{k})$ be a Dirac delta function at $\mathbf{n} = \mathbf{n}^o$. The reverse Fourier transform, $\Theta(\mathbf{r})$,

is then an infinitesimally thin plate perpendicular to $\mathbf{n}^o$. Mathematically,

$$\begin{aligned}\theta(\mathbf{r}) &= \int\theta(\mathbf{k})\exp(i\mathbf{k}\cdot\mathbf{r})d^3k/(2\pi)^3 \\ &= \int_0^{2\pi}d\beta\int_0^{\pi}\sin\alpha d\alpha\int\theta(\mathbf{k})\exp(i\mathbf{k}\cdot\mathbf{r})k^2dk/(2\pi)^3 \\ &= \int_0^{\pi}\sin\alpha d\alpha\int\theta(\mathbf{k})\exp(i\mathbf{k}\cdot\mathbf{r})k^2dk/(2\pi)^2 \\ &= \int\theta(\mathbf{k})\exp(i\mathbf{k}\cdot\mathbf{r})k^2dk/2\pi^2\end{aligned} \tag{2.2.3}$$

where α and β are the azimuthal and polar angles, respectively. $\theta(\mathbf{k})$ is zero unless $\mathbf{k}$ lies in a direction parallel to $\mathbf{n}^o$. The above integral is zero, then, unless

$$\mathbf{n}^o\cdot\mathbf{r} = 0. \tag{2.2.4}$$

Therefore, when the surface energy is negligible, the preferred shape is an infinitesimally thin plate whose habit plane $\mathbf{n}^o$ is determined by a minimization of $B(\mathbf{n})$.

When there is more than one value of $\mathbf{n}$ for which $B(\mathbf{n}) = B(\mathbf{n}^o)$, the preferred shape is still a thin plate. There will, however, be more than one habit plane. These variants are in general related by the symmetry of the crystal. For example, homogeneously-nucleated G-P zones form in Al-Cu alloys on the three {100} planes.

In the limit of an elastically isotropic system, there is no preferred shape when the elastic free energy is considered alone. For

an isotropic crystal,

$$B(\mathbf{n}) = B, \tag{2.2.5}$$

a constant independent of the direction $\mathbf{n}$. Equation (2.2.1) is then by definition an equality:

$$F_{el} = (V/2)B. \tag{2.2.6}$$

The elastic free energy is a constant independent of the shape of the precipitate. The preferred shape is then determined by a minimization of the surface energy.

2.2.2. Ellipsoidal Precipitates

2.2.2.1. Elastic Theory

For an ellipsoid, the shape function is given by

$$\Theta(\mathbf{k}) = 3V[\sin\phi(\mathbf{k}) - \phi(\mathbf{k})\cos\phi(\mathbf{k})]/[\phi(\mathbf{k})]^3 \tag{2.2.7}$$

where $\phi(\mathbf{k}) = (L_{ij}k_ik_j)^{1/2}$ and the eigenvalues of $\mathbf{L}$ are the squares of the ellipsoid semi-axes [1]. For a sphere, then,

$$L_{ij} = R^2\delta_{ij} \tag{2.2.8}$$

where R is the radius and δ_{ij} is the Kronecker delta. Plugging in for

L in the expression for $\phi(\mathbf{k})$ gives

$$\phi(\mathbf{k}) = R\mathbf{k}. \tag{2.2.9}$$

Breaking the integral in equation (2.1.34) into one over the magnitude and one over the direction of $\mathbf{k}$, the elastic free energy may be written in the form

$$F_{el} = (1/2)\int_0^{2\pi}\int_0^{\pi} B(\mathbf{n}) \sin\alpha d\alpha d\beta \int |\Theta(\mathbf{k})|^2 k^2 dk/(2\pi)^3 \tag{2.2.10}$$

where α and β are the azimuthal and polar angles, respectively. Plugging equation (2.2.9) into the integral over the magnitude of k in the above equation yields

$$\int |\Theta(\mathbf{k})|^2 k^2 dk/(2\pi)^3 = [V^2/(2\pi)^3]\int k^2 |[\sin(kR) - kR\cos(kR)]/(kR)^3|^2 dk. \tag{2.2.11}$$

If the right hand side of the above equation is denoted by I, then by definition,

$$\begin{aligned} \int |\Theta(\mathbf{k})|^2 d^3k/(2\pi)^3 &= V \\ &= \int d\omega I \end{aligned} \tag{2.2.12}$$

where ω is the solid angle. Integration over the solid angle then gives

$$4\pi I = V$$

or (2.2.13)

$$I = V/4\pi .$$

For the special case of a spherical inclusion, then, the elastic free energy may be found by integration of B(**n**) over the solid angle:

$$F_{el}^{sphere} = (1/2) \int_0^{2\pi}\int_0^{\pi} B(\mathbf{n}) \sin\alpha d\alpha d\beta \ (V/4\pi)$$

$$= (V/8\pi) \int_0^{2\pi}\int_0^{\pi} B(\mathbf{n}) \sin\alpha d\alpha d\beta . \qquad (2.2.14)$$

The reason for considering a spherical inclusion is now evident. Because the integral over the magnitude of **k** may be solved analytically, the problem of numerical integration is greatly simplified. Khachaturyan [1] uses this result for a general ellipsoid by transforming the coordinates so that the ellipsoid becomes a sphere. Plugging in this coordinate transformation, equation (2.2.14) becomes

$$F_{el} = (V/8\pi) \int_0^{2\pi}\int_0^{\pi} B[\mathbf{n}(\mathbf{n}')] \sin\alpha d\alpha d\beta \qquad (2.2.15)$$

where

$$n_i(\mathbf{n}') = L_{ij}^{-1/2} n_j' / (n_i' L_{ij}^{-1} n_j')^{1/2} . \qquad (2.2.16)$$

2.2.2.2. Approach to Computer Calculations

The shape of a precipitate, its habit plane and the orientation relations between its lattice and that of the matrix are of course

interrelated. The solution to a problem which leaves all three of these factors variable, however, would at best be difficult to obtain. As a first step toward this final goal, the orientation relations and the habit plane are assumed to be those seen experimentally so the equilibrium shape may be calculated relatively simply. In other words, the matrix and precipitate axes are assumed parallel and an (001) habit plane is assumed. Also, only ellipsoids of revolution about the [001] axis are considered.

Rewriting L in terms of volume and aspect ratio, K (defined as the semi-axis in the habit plane over the unique semi-axis along the [001] direction, a/c), it is easily shown that the coordinate transformation, equation (2.2.16), may be written in the following form:

$$n_i(\mathbf{n}') = [n_j'\delta_{ij} + (K-1)n_3'\delta_{i3}]/[(n_1')^2 + (n_2')^2 + (Kn_3')^2]^{1/2}. \quad (2.2.17)$$

$B(\mathbf{n}')$ depends only on the elastic constants and the crystal structures of the precipitate and matrix phases. It does not depend on precipitate shape. As a result, $B(\mathbf{n}')$ need be calculated only once for each system investigated. These values are placed in a table which is referred to for calculations at any aspect ratio.

Calculation of $B(\mathbf{n}')$ is fairly straightforward. The components of $\mathbf{n}'$ in terms of the integration parameters, α and β, are given by

$$\begin{aligned} n_1' &= \sin\alpha\cos\beta \\ n_2' &= \sin\alpha\sin\beta \\ n_3' &= \cos\alpha. \end{aligned} \quad (2.2.18)$$

In this investigation, a cubic transformation has been assumed. The stress-free transformation strain may then be written in the form

$$\varepsilon^{o}_{ij} = \delta_{ij} \quad (\varepsilon^{o}) \tag{2.2.19}$$

where ε^{o} is a constant and is a measure of the dilation. Here, the symbols in parentheses to the right of the equations are factored out of the calculation in order to nondimensionalize it. For cubic systems, the elastic stiffness tensor may be written as

$$\lambda_{ijkl} = (\delta_{ik}\delta_{jl} + \delta_{il}\delta_{jk} + C_2\delta_{ij}\delta_{kl} + \Delta\delta_{ij}\delta_{jk}\delta_{kl}) \quad (C_{44}) \tag{2.2.20}$$

where

$$\Delta = (C_1 - C_2 - 2) \quad (C_{44}) \tag{2.2.21}$$

is the anisotropy factor and

$$\begin{aligned} C_1 &= C_{11}/C_{44} \\ C_2 &= C_{12}/C_{44}. \end{aligned} \tag{2.2.22}$$

In the final equation, the constant $C_{44}\varepsilon_o^2$ is factored out. Note that this constant has units of energy per unit volume. If actual energy values were desired, then the dimensionless energy must be multiplied by $C_{44}\varepsilon_o^2$. The transformation stress and the dynamical matrix tensor is now found using equations (2.1.13) and (2.1.30),

respectively, and the incremental energies,

$$B(\mathbf{n}') = \sigma_{ij}^{o}\delta_{ij} - n_i'\sigma_{ij}^{o}\Omega_{jk}\sigma_{kl}^{o}n_l' \qquad (C_{44}\varepsilon_o^2), \qquad (2.2.23)$$

are tabulated as a function of α and β. The main program reads in an aspect ratio and numerically integrates equation (2.2.15) over α and β. First, $\mathbf{n}'$ is found by equation (2.2.18) and substituted into the coordinate transformation, equation (2.2.17). The transformed values of α and β, α' and β', are then calculated from $\mathbf{n}(\mathbf{n}')$. Given these, $B[\mathbf{n}(\mathbf{n}')]$ is then calculated by a second-order Taylor expansion about the values α and β in the 'look-up' table nearest to α' and β'.

The elastic constants used [25-27] in the elastic free energy calculations are given in Table 1. The results using the elastic constants for γ' (Ni_3Al) are displayed graphically in Figure 3. The form of this curve is similar for all elastic constants used. The elastic free energy is maximum for a sphere and approaches an absolute minimum as K approaches infinity (i.e. an infinitesimally thin plate).

2.2.3. Cuboidal Precipitates

In real space, the shape function for a cube of side L is given by

$$\Theta(\mathbf{r}) = \begin{cases} 1 & -L/2<x<L/2,\ -L/2<y<L/2,\ -L/2<z<L/2 \\ 0 & \text{otherwise.} \end{cases} \qquad (2.2.24)$$

Taking the Fourier transform,

$$\theta(\mathbf{k}) = \int\theta(\mathbf{r})\exp(-i\mathbf{k}\cdot\mathbf{r})d^3r$$

$$= \int_{-L/2}^{L/2} \exp(-ik_1x)dx \int_{-L/2}^{L/2} \exp(-ik_2y)dy \int_{-L/2}^{L/2} \exp(-ik_3z)dz \tag{2.2.25}$$

where x, y, and z are the components of **r** along the [100], [010] and [001] axes, respectively, and k_1, k_2, and k_3 are the Fourier components. The three integrals above are identical in form; solving only the one over x:

$$\int_{-L/2}^{L/2} \exp(-ik_1x)dx = \int_{-L/2}^{L/2} [\cos(k_1x) - i\sin(k_1x)]\, dx$$

$$= \sin(k_1x)/k_1 \,\Big|_{-L/2}^{L/2} + i\cos(k_1x)/k_1 \,\Big|_{-L/2}^{L/2} \tag{2.2.26}$$

$$= 2\sin(k_1L/2)/k_1.$$

Substituting into equation (2.2.25),

$$\theta(\mathbf{k}) = 8[\sin(k_1L/2)/k_1][\sin(k_2L/2)/k_2][\sin(k_3L/2)/k_3]$$

$$= 8V[\sin(k_1L/2)/k_1L][\sin(k_2L/2)/k_2L][\sin(k_3L/2)/k_3L]. \tag{2.2.27}$$

This shape function could be substituted into equation (2.1.34) to obtain the strain energy. Unlike the sphere, however, the shape function for a cube depends on both the magnitude and the direction of **k**. A straightforward analytical solution for the integration over the magnitude of **k** is not possible. This fact makes numerical integration

of equation (2.1.34) both time consuming and costly.

Fortunately, a very good approximation for the incremental elastic free energy has been derived by Khachaturyan [1]. This approximation applies to the particular case where both the precipitate and matrix crystal structures are cubic. Using this approximation, the incremental free energy may be written as

$$B(\mathbf{n}) = (C_1+2C_2)\{\ 2(C_1-C_2)/C_1 - 4\Delta(C_1+2C_2)/[C_1(C_1+C_2+2)](n_1^2n_2^2+n_2^2n_3^2+n_3^2n_1^2) \tag{2.2.28}$$

$$- 54\Delta^2(C_1+2C_2)/[C_1(C_1+C_2+2)(C_1+2C_2+4)](n_1^2n_2^2n_3^2)\}\quad (C_{44}\varepsilon_o^2V).$$

Substitution of equations (2.2.27) and (2.2.28) into equation (2.1.34) for the elastic free energy yields:

$$F_{el}^{cube} = (1/2)(C_1+2C_2)\ \{\ 2(C_1-C_2)/C_1 - 4I_1\Delta(C_1+2C_2)/[C_1(C_1+C_2+2)] \tag{2.2.29}$$

$$- 54I_2\Delta^2(C_1+2C_2)/[C_1(C_1+C_2+2)(C_1+2C_2+4)]\}\quad (C_{44}\varepsilon_o^2V)$$

where, using the definition $n_i^2 = k_i^2/(k_1^2+k_2^2+k_3^2)$ and solving numerically,

$$I_1 = V \int [(k_1^2k_2^2+k_1^2k_3^2+k_2^2k_3^2)/(k_1^2+k_2^2+k_3^2)^2]$$

$$\times [\sin^2(k_1L/2)/(k_1L/2)^2] [\sin^2(k_2L/2)/(k_2L/2)^2]$$

$$\times [\sin^2(k_3L/2)/(k_3L/2)^2] dk_1dk_2dk_3/(2\pi)^3$$

$$= 8 \int [(x^2y^2+x^2z^2+y^2z^2)/(x^2+y^2+z^2)^2] (\sin^2x/x^2) \qquad (2.2.30)$$

$$\times (\sin^2y/y^2) (\sin^2z/z^2) dxdydz/(2\pi)^3$$

$$= 24 \int [\sin^2x\sin^2y\sin^2z/z^2(x^2 + y^2 + z^2)] dxdydz/(2\pi)^3$$

$$= 0.15784$$

and

$$I_2 = V \int [k_1^2k_2^2k_3^2/(k_1^2+k_2^2+k_3^2)^3]$$

$$\times [\sin^2(k_1L/2)/(k_1L/2)^2] [\sin^2(k_2L/2)/(k_2L/2)^2]$$

$$\times [\sin^2(k_3L/2)/(k_3L/2)^2] dk_1dk_2dk_3/(2\pi)^3 \qquad (2.2.31)$$

$$= 8 \int [\sin^2x\sin^2y\sin^2z/(x^2 + y^2 + z^2)^3] dxdydz/(2\pi)^3$$

$$= 0.007664.$$

3. The Surface Energy

Because the surface to volume ratio is large when the precipitates are small, the surface energy is dominant at small precipitate volumes. When γ' precipitates are small, they are generally spherical in shape implying an isotropic surface energy at least in the early stages of precipitation and growth. If later during coarsening, the γ' precipitates changed to a cuboidal shape due to an anisotropic surface energy then it might be expected that they form initially as cubes when the surface energy is dominant. Since this is not generally observed, an isotropic surface energy is assumed for all precipitate volumes.

3.1. The Surface Energy of an Ellipsoidal Precipitate

The surface area for an ellipsoid of revolution is given by

$$S^{ellip} = (8\pi/3)a^2 + (4\pi/3)a_3^2 \qquad (3.1.1)$$

where a_3 is the unique semi-axis and $a = a_1 = a_2$ are the semi-axes in the habit plane. Rewriting this area in terms of the volume and aspect ratio yields

$$S^{ellip} = (4\pi/3)^{1/3}V^{2/3}[2K^{2/3} + K^{-4/3}]. \qquad (3.1.2)$$

The isotropic surface energy is therefore given by

$$F_{surf}^{ellip} = \gamma(4\pi/3)^{1/3}V^{2/3}[2K^{2/3} + K^{-4/3}] \qquad (3.1.3)$$

where γ is the surface tension.

In order that the elastic and surface energies may be added together, the constant $C_{44}\varepsilon_o^2V$ is factored out to give:

$$F_{surf}^{ellip} = (4\pi/3V)^{1/3}(\gamma/C_{44}\varepsilon_o^2)[2K^{2/3} + K^{-4/3}]\ (C_{44}\varepsilon_o^2V)$$

$$= g\ [2K^{2/3} + K^{-4/3}]\ (C_{44}\varepsilon_o^2V) \qquad (3.1.4)$$

where

$$g = (4\pi/3V)^{1/3}[\gamma/C_{44}\varepsilon_o^2] \qquad (3.1.5)$$

and will be called the surface energy constant.

The surface energy is shown in Figure 4 for different values of the surface energy constant as a function of aspect ratio. As expected, the surface energy is minimum for a sphere and increases at a given aspect ratio with g.

3.2. The Surface Energy of a Cuboidal Precipitate

The surface energy of a cube is given by

$$F_{surf}^{cube} = 6\gamma L^2 \qquad (3.2.1)$$

where L is the length of the cube edge. Again factoring out $(C_{44}\varepsilon_o^2V)$ gives

$$F_{surf}^{cube} = 6(\gamma/C_{44}\varepsilon_o^2)\ L^2/V\ (C_{44}\varepsilon_o^2 V). \tag{3.2.2}$$

Rewriting in terms of the surface energy constant, g:

$$F_{surf}^{cube} = 6\ (3/4\pi)^{1/3}\ (4\pi/3V)^{1/3}\ (\gamma/C_{44}\varepsilon_o^2)\ L^2/L^2\ (C_{44}\varepsilon_o^2 V)$$

$$= 6\ (3/4\pi)^{1/3}\ g\ \ (C_{44}\varepsilon_o^2 V). \tag{3.2.3}$$

4. The Preferred Shape

The preferred shape of an isolated precipitate is determined by a balance between the strain and surface energies. This total free energy is shown for a γ' precipitate (i.e. meaning the γ' elastic constants were used to calculate the elastic free energy) as a function of aspect ratio in Figure 5. At small values of g, the absolute minimum in the free energy corresponds to precipitates with a plate shape. A spherical precipitate would have a locally maximum value in the free energy. As g increases, the absolute minimum moves to smaller aspect ratios and to free energy values which increase relative to the values for an aspect ratio K=1. Meanwhile a local minimum develops for a sphere, and beyond a certain value of g becomes the absolute minimum in the free energy. At relatively large values of g, the local minimum for a plate disappears, and the shape of the total free energy curve is dominated by that of the isotropic surface energy. These qualitative results for the ellipsoid model are summarized more clearly in Figure 6 where the preferred aspect ratio (i.e. that which minimizes the free energy) is plotted as a function of g.

The free energy of the preferred shape determined by the ellipsoid model and of the cube are plotted as a function of g in Figure 7. At a given value of g, the free energy plotted for the ellipsoid is the absolute minimum in the free energy at that value of g. The corresponding shapes are therefore plates at small values of g and spheres when g is relatively large. The cube model resulted in a single value of the strain energy. Hence, the total free energy is linear in g. From this curve, it can be seen that the equilibrium

shape of a cubic precipitate in a cubic matrix is a plate for small values of g, a cube at intermediate values, and a sphere at relatively large values of g. These results then agree, at least qualitatively, with experimental observations since g is inversely proportional to the cube root of the volume.

5. Numerical Results

The intersections of the two curves in Figure 7 determine where the transitions in shape are expected to occur. These intersections are designated by the critical values of g: g_c for the sphere to cube transition and g_p for the cube to plate transition. The values of g_c and g_p obtained for the systems investigated are given in Table 2.

By the definition of g, equation (3.1.5), increasing the surface tension γ or decreasing the misfit ε^o and the volume of the precipitate V increases g. All of these will therefore have an effect on the preferred shape. Here, only the effect of precipitate volume will be considered directly so that the results may be compared to experimentally observed shape changes during coarsening.

In order to directly compare these results with experiment, it is desirable to solve equation (3.1.5) for $V^{1/3}$ which will be called the characteristic diameter, d:

$$d=(4\pi/3)^{1/3}\ [\gamma/C_{44}\varepsilon_o^2 g]. \tag{5.1}$$

The experimental values of γ, C_{44} and ε_o are needed to solve this equation. The value of C_{44} used [25-27] for each of the systems investigated are shown in Table 1, and the misfits used are shown in Table 3. The surface tension of the alloy systems investigated have been measured using the Lifshitz-Sloyozov-Wagner (LSW) coarsening theory [28-30]. Since the accuracy of these results can only be as good as the theory used to get them, the surface tension values are approximate. For the Ni-Al and Al-Li systems, the surface tension is

on the order of 10 erg/cm^2; for γ' in Ni-Ti alloys, it is approximately 20 erg/cm^2.

In these types of calculations, it is important to be aware of how the misfit is measured. The use of precipitate lattice parameters which are measured say by x-ray diffraction of a bulk sample are inappropriate here since they are the constrained precipitate lattice parameters. Unconstrained lattice parameters may be found, for example, by extracting the precipitates and doing powder x-ray diffraction.

The Ni-Al system is relatively easy to investigate because the Ni_3Al precipitate is an equilibrium phase. Corey and Lisowsky [31] have measured the lattice parameter of a single-phase Ni_3Al sample. Ardell's [28] surface tension work was done on a Ni-6.5 wt.% Al alloy. From the equilibrium Ni-Al phase diagram published by Hansen and Anderko [32], a γ' precipitate in an alloy of this composition contains about 11 wt.% Al. Unfortunately, Corey and Lisowsky do not measure the lattice parameter of single-phase Ni_3Al with 11 wt.% Al. They do, however, report a value of 3.571Å for the lattice parameter of a sample with 14 wt.% Al. Also from the Ni-Al phase diagram at a 700°C aging temperature, the Ni matrix contains about 5 wt.% Al. From the lattice parameter measurements of Corey and Lisowsky [31], a Ni-5 wt.% Al solid solution has a lattice parameter of 3.541 Å. Using these values, the stress-free transformation strain for this system is about 0.0085.

Unfortunately, Ni_3Ti is only a metastable phase, and its lattice parameter has not been directly measured. Mihalisin and Decker [33] measured the lattice parameter of Ni_3Ti in a bulk Ni-9.1 wt.% Ti alloy, but it is unclear whether these precipitates are constrained or not.

Since they etch the bulk sample to bring the γ' precipitates into relief, it is possible that the precipitates are unconstrained. Using x-ray diffraction, they then obtain a lattice parameter of 3.589 Å for the Ni_3Ti phase. Taylor and Floyd [34] measured the matrix lattice parameter for alloys of similar composition to be 3.549 Å. Using these values, the stress-free transformation strain is 0.011.

Sass et al. [35] calculated the image of a cubical γ' precipitate in a TEM microscope and measured what they called image widths as a function of the stress-free transformation strain. They then measured the image width of an experimentally observed γ' precipitate in a Ni - 8 wt.% Ti - 0.3 wt.% Al alloy and compared it to the calculated values to obtain a stress-free transformation strain of 0.0085. Since the unconstrained precipitate lattice parameter will yield a greater strain than that of the constrained precipitate, the etched precipitates of Mihalisin and Decker [33] are likely to have been unconstrained and a transformation strain of 0.011 is used here.

The δ' misfit has been measured by several authors [36-39] using the method of Ashby and Brown [40] who calculated the image width of a precipitate as a function of the constrained strain. The reported values lie between -0.0008 and -0.0012. Unfortunately, the unconstrained δ' lattice parameter has not been measured. The exact value of the stress-free transformation strain, however, is not necessary in this case. Because δ' precipitates are never seen to take on a cuboidal shape, only a rough estimate is needed for the transition size. For this reason, the stress-free transformation strain will be calculated from the constrained strain, ε_c, using the equation:

$$\varepsilon_o = 1.5\varepsilon_c \tag{5.2}$$

taken from Eshelby [11] who assumed that the matrix and precipitate elastic constants were the same and that Poisson's ratio , $\upsilon=1/3$. Using equation (5.2), the stress-free transformation strains are between -0.0012 and -0.0018. Here, a value of -0.0015 will be used.

These values were used in equation (5.1) to determine the critical particle sizes for the cube and plate shape transitions. The results are shown in Table 4.

6. Discussion

The stress-free transformation strain varies considerably with the composition of the alloy. Since this quantity goes into the critical particle size calculation squared, it is important to compare the theoretical results to sizes observed in alloys with compositions similar to that from which the strain was taken. The surface tension does not seem to be as important since it does not change much with composition and only goes into the calculation to the first power.

6.1 The Sphere to Cube Transition

The results for the Ni-Al system are in good agreement with experimental observations. Cuboidal γ' precipitates have been observed at sizes as small as 50 Å in these alloys. Phillips [41] observed γ' precipitates using dark-field TEM as small as 25 Å in diameter. The shape of the precipitates was determined to be cuboidal at sizes greater than about 50 Å by direct observation in dark-field TEM and by analyzing strain field contrast effects in bright-field TEM.

Unfortunately, γ' cubes have not been reported at such small particle sizes in Ni-Ti systems simply because no one has attempted to observe the shape at small precipitate sizes. It is likely that a method such as that used by Phillips [41] would reveal that the γ' precipitates in Ni-Ti alloys are cuboidal in shape at the smaller sizes. In fact, the micrographs shown by Sass et al. [35] seem to suggest that they are.

The results for the Al-Li system are in excellent agreement with

experimental observations in that δ′ particles are, at least on a macroscopic level, always spherical in shape. The largest δ′ precipitate observed without coalescence is about 0.2–0.3 μm in diameter [42,43]. This size corresponds to a characteristic diameter, d, of 0.16–0.24 μm which is well below the predicted critical value of 3.1 μm where the sphere is no longer stable with respect to formation of a cube.

6.2. The Cube to Plate Transition

Before comparing the results for the cube to plate transition, the mechanism by which plates form in practice and that used in the model must be considered. Recall that the critical particle sizes were calculated from the value of the surface energy constant where the total free energy curves for the ellipsoid and cube intersected. A single value of g and, hence, a single value of the precipitate volume was obtained for each shape transition. In other words, the transitions for which the critical particle sizes are calculated are ones which occur by a constant-volume process. For example, the cube to plate transition is modeled as a cube flattening out at constant volume along one pair of the {100} faces.

In practice, the sphere to cube transition is essentially a constant-volume process. The γ′ spheres flatten out on the {100} faces to become globules with no well defined shape. These globules then become more and more cuboidal in shape. The cube to plate transition, on the other hand, is clearly not a constant-volume process in practice. As stated previously, what actually happens in practice is

that the γ' cubes line up and move together along the ⟨100⟩ directions in the Ni matrix. This process is shown schematically in Figure 8 where the constant-volume process is also shown for comparison.

The theoretical calculations made in this investigation have been for an isolated precipitate. As the γ' cubes in practice approach each other, eventually they must reach a point where they can no longer be considered to be isolated. There is an interaction energy which must be accounted for. In fact, it is this interaction energy that is responsible for the cubes lining up in the first place. The effect of the interaction energy will be to lower the free energy of the aligned cubes so that it presumably becomes less than the plate energies at larger volumes than predicted.

No matter how it forms, however, a plate-shaped precipitate once it has formed should not be stable below the characteristic diameters shown in Table 4. For an isolated precipitate, this means that unless the cube shape is metastable, a cuboidal γ' precipitate in a Ni-Al alloy, for example, must begin to flatten out becoming a plate when its edge length becomes 130 Å. If the cuboid only becomes metastable (as opposed to unstable), then, for kinetic reasons, the shape may not change until sizes well above 130 Å.

For the interacting cuboidal γ' precipitates discussed previously, plates may not form until sizes much larger than those predicted for a couple of reasons. First, while the plate is stable with respect to an isolated cube of the same volume, it may not be stable with respect to an array of cubes each with a fraction of its volume. In other words, an array of interacting cuboidal precipitates is likely to have a lower free energy than an isolated cuboid with the total volume of all the

cubes in the array. Second, the aligned cubes may not, once coalesced, form a plate with the preferred or nearly preferred aspect ratio associated with that precipitate volume. This may explain why γ' cubes often move very close together even becoming distorted in shape [6,44] without coalescing. It is possible that a plate with the aspect ratio formed by coalescence of the cuboids has a free energy greater than that of the aligned cuboids.

Both Ardell and Nicholson [6] and Gleiter and Hornbogen [7] have published micrographs of plate-shaped γ' precipitates in Ni ~6 wt.% Al alloys with characteristic diameters of about 0.2 μm. From equation (3.1.5), a value of g of about 0.010 corresponds to this volume. From data similar to that plotted in Figure 6, the preferred aspect ratio at this value of g is about 24. The aspect ratios of the micrographed plates [6,7] vary from about 4 to 11. While these aspect ratios are much lower than the preferred aspect ratio at this value of g, the free energies of the corresponding plates are still below that of a cube with the same volume. It is therefore likely that these plates are more stable than the arrangement of cubes that preceded them and have simply not had enough time kinetically to flatten out to the preferred aspect ratio.

Some of the γ' plates reported prior to the mid 1960's may actually have been γ''. γ'' is an ordered tetragonal phase and, for reasons given in Appendix 5, is never spherical in shape. In practice, γ'' always forms as plates and remains plate-shaped throughout coarsening.

6.3 The Effect of Anisotropy and Misfit on the Critical Particle Sizes

In Table 4, the Al-Li system stands out in that its critical particle sizes, d_c, are much larger by a few orders of magnitude than those for the other systems investigated. There are likely to be several causes for this large difference. The most likely cause is the relative isotropy of the Al matrix. The anisotropy factors for the three systems investigated are shown in Table 5. The anisotropy of Al is much closer in magnitude to zero than that for either Ni or γ'. Since it is reasonable to assume that increasing the elastic isotropy of the system would increase the stability of a spherical precipitate, the effect of elastic anisotropy on the critical particle size for the sphere to cube transition was investigated.

In order to study the effect of anisotropy alone, the Lamé constants,

$$\lambda=C_1+2C_2 \quad (C_{44}) \tag{6.4.1}$$

and

$$\mu = 1 \quad (C_{44}) \tag{6.4.2}$$

were fixed at the values for Al. The critical particle sizes for the cube transition are shown in Table 6 for several values of the anisotropy factor. As expected, the critical sizes decrease as the magnitude of the anisotropy factor increases. Even at relatively large anisotropy factors, however, the critical sizes are still not as small as those found using the Ni and γ' elastic constants.

Another possible explanation has to do with the relatively low

misfit of δ′ in Al. Since the characteristic diameter, d, is inversely proportional to the square of the magnitude of the stress-free transformation strain, it is reasonable to assume that the misfit has a relatively large effect on the critical particle sizes. In order to verify this assertion, d_c was calculated using the Al data but substituting in larger misfits. These results are shown in Table 7 where it can be seen that increasing the δ′-Al misfit dramatically decreases d_c. When the misfit is comparable to that for the other systems, however, d_c is still much larger.

As seen in Tables 6 and 7, both the anisotropy factor and the δ′-Al misfit have an effect on the stability of the spherical shape. The misfit has a stronger effect, but neither alone is enough to explain the relatively large critical particle sizes for δ′ in Al. It is likely that both acting together are the reason for the relative stability of spherical δ′ precipitates with the relatively low misfit being the stronger effect.

6.4 The Validity of the Homogeneous Elastic Constants Assumption

The assumption of homogeneous elastic constants seems to be a very strong assumption, but in many cases, it can be appropriate. It is often claimed that the assumption is reasonable provided the anisotropy factors of the precipitate and matrix phases are similar. Clearly, the anisotropy factor has a relatively large effect on the elastic free energy. This was demonstrated in the previous subsection. As shown in Table 5, the anisotropy factors for γ′ and Ni are nearly the same, and as shown in Table 4, the critical particle sizes obtained for the Ni-Al

system using either the γ' or the Ni elastic constants were virtually identical. Therefore, the assumption of homogeneous elastic constants seems quite reasonable at least for the Ni-Al system. It might also be expected that the assumption is valid for the Ni-Ti system assuming Ni_3Al and Ni_3Ti are elastically similar.

The validity of the homogeneous elastic constants assumption for the Al-Li system, on the other hand, is questionable. The elastic constants of δ' can't be measured using conventional methods because δ' is not a stable phase. And without knowing these constants, it is impossible to be certain whether or not they are similar to those of Al.

It is sometimes asserted that most of the strain due to the difference in the precipitate and matrix lattices is present in the precipitate. If this were the case, then the assumption of homogeneous elastic constants would be valid provided the elastic constants of the precipitate were used. Since the precipitate elastic constants are seldom known, the elastic constants of the matrix are then used. In the case of Al-Li, however, even if most of the strain were in the δ' precipitates, it might not be reasonable to expect that δ' be quite so elastically isotropic as Al.

Recently Muller et al. [45] have measured the δ' elastic constants using a revolutionary technique. They have developed a theory by which they can infer the precipitate elastic constants from ultrasonic pulse echo measurements made through a single crystal containing precipitates given the matrix elastic constants. Their results are quite surprising. They found that the anisotropy factor for δ', while negative at room temperature, is positive at the typical aging

temperatures.

The results of the work done by Wen et al. [21] state that cubic systems with a dilatational transformation strain will precipitate plates on a {100} habit plane if the anisotropy factor is negative and on a {111} habit plane if it is positive. As a result, it is reasonable to expect that γ' cubes will form because the faces of the cubes lie on {100} planes. If the anisotropy factor of δ' is positive, however, then δ' may not be reasonably expected to form cubes because the {100} planes would no longer be the planes of lowest elastic energy. A shape such as a tetrahedron might be more reasonable.

The technique used by Muller et al. to measure the δ' elastic constants, however, is new and, as yet, untested. It might be interesting, for example, if the Ni_3Al elastic constants were measured with the technique used by Muller et al. and compared to the known values. In any case, δ' is unlikely to form as cubes. Whether it does not because the Al-Li system is almost isotropic and has a low misfit or whether δ' has a positive anisotropy factor is unclear.

7. Conclusions

The theoretical results presented here for homogeneous precipitation are in excellent qualitative agreement with experimental observations. The γ' phase was predicted to form as spheres and change shape to cubes and plates during coarsening. Good quantitative agreement was achieved when reasonable values of the precipitate-matrix misfit, surface tension and elastic constants were used. For a Ni alloy with about 6 wt.% Al, this transition was found to occur at about 110 Å. For a Ni ~9 wt.% Ti alloy, this transition was predicted to occur at about 130 Å. A spherical δ' precipitate in a typical Al-Li alloy was not predicted to change to a cuboidal shape until its characteristic diameter reached 3 μm.

The cube to plate transition can occur by two processes: 1) by a constant-volume flattening of an isolated cube on one pair of the six {100} faces and 2) by the coalescence of interacting cubes lined up in ⟨100⟩ directions on a {100} plane. The theoretical model presented here applies to the constant-volume process and predicts a transition size of 130 to 200 Å for γ' in the Ni-Al and Ni-Ti alloys and of 8.5 μm for δ' in the Al-Li alloys. No plate-shaped precipitates should be stable below these sizes, and none have been reported. For kinetic reasons, the actual shape transition may not occur until well above these values if the cuboidal shape is metastable with respect to the plate shape. The metastability of the cube, however, cannot be tested by the model used here.

The size of a precipitate at the cube to plate transition occurring by the second process named, which is what is seen

experimentally in alloys of normal precipitate volume fraction, can be anything above the critical values for the constant-volume process provided the aspect ratio is one which makes the plate energy less than that of the aligned cubes. If coalescence of the array of cubes were to produce a plate with an unfavorable combination of volume and aspect ratio, then the cubes would not coalesce no matter how close together they got.

The predicted shape transition sizes for δ′ in Al-Li alloys were several orders of magnitude larger than those for γ′ in the Ni alloys. The stability of spherical δ′ was found to be due to a combination of the relative isotropy of Al and the relatively low δ′-Al misfit with the misfit effect being the stronger of the two. Experimentally, these effects play a part in the stability of δ′ spheres; but the possibility that δ′ has a positive anisotropy factor making the cube shape undesirable may also be a factor.

Based on the results of this theoretical investigation, the homogeneous elastic constants assumption seems to be reasonable for the γ′- Ni-Al and γ′- Ni-Ti systems. For δ′ in Al-Li, however, the validity of this assumption is at best questionable.

REFERENCES

1. A.G. Khachaturyan, Theory of Structural Transformations in Solids, John Wiley and Sons, Inc., New York, (1983).
2. J. Glazer, M.S. Thesis, University of California, Berkeley, CA (1986).
3. C.P. Sullivan and M.J. Donachie, Jr. in "Source Book on Materials for Elevated-Temperature Applications," ed. by E.F. Bradley, ASM, Metals Park, Ohio, 239 (1979).
4. R.F. Decker in "Source Book on Materials for Elevated-Temperature Applications," ed. by E.F. Bradley, ASM, Metals Park, Ohio, 275 (1979).
5. G.H. Narayanan, W.E. Quist, B.L. Wilson and A.L. Wingert, "Low-Density Aluminum Alloy Development," First Interim Technical Report Jan. 4, 1982-July 1, 1982. AFWAL contract F33615-81-C-5033, Aug., 1982.
6. A.J. Ardell and R.B. Nicholson, Acta Met., 14 (1966), 1295.
7. H. Gleiter and E. Hornbogen, Mat. Sci. Eng., 2 (1968), 285.
8. A.G. Khachaturyan, Sov. Phys. Solid State, 8 (1967), 2163.
9. J.D. Eshelby, Proc. Roy. Soc. A, 241 (1957), 376.
10. J.D. Eshelby, Proc. Roy. Soc. A, 252 (1959), 561.
11. J.D. Eshelby in "Progress in Solid Mechanics", vol. 2, ed. by I.N. Sneddon and R. Hill, North Holland Publishing Co., Amsterdam, 89 (1961).
12. L.J. Walpole, Proc. Roy. Soc. A, 300 (1967), 270.
13. N. Kinoshita and T. Mura, Phys. Status Sol., 5(a) (1971), 1379.
14. J.K. Lee, D.M. Barnet and H.I. Aaronson, Met. Trans., 8A (1977),

963.

15. J.D. Boyd and R.B. Nicholson, Acta Met., 19 (1971), 1379.

16. T. Miyazaki, H. Imamura and T. Kozakai, Mat. Sci. and Eng., 54 (1982), 9.

17. M. Doi, T. Miyazaki and T. Wakatsuki, Mat. Sci. and Eng., 67 (1984), 247.

18. M. Hong, M.S. Thesis, University of California, Berkeley, CA (1978).

19. S.H. Chen, Ph.D. Thesis, University of California, Berkeley, CA (1979).

20. D.E. Wedge, M.S. Thesis, University of California, Berkeley, CA (1980).

21. S.H. Wen, E. Kostlan, M. Hong, A.G. Khachaturyan and J.W. Morris, Jr., Acta Met., 29 (1981), 1247.

22. M. Hong, D.E. Wedge and J.W. Morris, Jr., Acta Met., 32 (1984), 279.

23. J.W. Morris, Jr., A.G. Khachaturyan and S.H. Wen, Lawrence Berkeley Laboratory Report No. 9800, Berkeley, CA (1981).

24. J.W. Morris, Jr., A.G. Khachaturyan and S.H. Wen in "Proceedings of the NATO Advanced Study Institute on Modulated Structure Materials," ed. by T. Tsakalakos, Mortinus Nijhoff, Holland, 327 (1984).

25. K. Ono and R. Stern, Trans. AIME, 245 (1969), 171.

26. J. de Klerk and M.J.P. Musgrave, Proc. Phys. Soc. (London), B68 (1955), 81.

27. H.B. Huntington, Solid State Phys., 7 (1958), 213.

28. A.J. Ardell, Acta Met., 16 (1968), 511.

29. A.J. Ardell, Met. Trans., 1 (1970), 525.

30. S.F. Baumann and D.B. Williams, Scripta Met., 18 (1984), 611.

31. C.L. Corey and B. Lisowsky, Trans. AIME, 239 (1967), 239.

32. M. Hansen and K. Anderko, Constitution of Binary Alloys, McGraw-Hill Book Co., New York, 118 (1958).

33. J.R. Mihalisin and R.F. Decker, Trans. AIME, 218 (1960), 507.

34. A. Taylor and R.W. Floyd, J. Inst. Metals, 80 (1951-52), 577.

35. S.L. Sass, T. Mura, and J.B. Cohen, Phil. Mag., 16 (1967), 679.

36. D.B. Williams and J.W. Edington, Met. Sci., 9 (1975), 529.

37. S.F. Baumann and D.B. Williams in "Aluminum-Lithium Alloys II," ed. by T.H. Sanders and E.H. Starke, Jr., AIME, New York, 17 (1983).

38. P. Sainfort and P. Guyot in "Aluminum-Lithium Alloys III," ed. by C. Baker, P.J. Gregson, S.J. Harris and C.J. Peel, Oxford, England, 420 (1985).

39. B. Noble and G.E. Thompson, Met. Sci., 5 (1971), 114.

40. M.F. Ashby and L.M. Brown, Phil. Mag., 8 (1963), 1083.

41. V.A. Phillips, Acta Met., 14 (1966), 1533.

42. D.B. Williams and J.W. Edington, Met. Sci., 9 (1975), 529.

43. T. Yoshi-yama, K. Hasebe and M. Mannami, J. Phys. Soc. Jpn., 25 (1968), 908.

44. T. Miyazaki, K. Nakamura and H. Mori, J. Mater. Sci., 14 (1979), 1827.

45. W. Muller, E. Bubeck and V. Gerold in "Aluminum-Lithium Alloys III, ed. by C. Baker, P.J. Gregson, S.J. Harris and C.J. Peel, Oxford, England, 435 (1985).

TABLE 1

Elastic Constants (in 10^{12}dyne/cm^2) Used in the Strain Energy Calculations

System	C_{11}	C_{12}	C_{44}	Reference
γ'	1.978	1.265	1.178	25
Ni	2.436	1.494	1.196	26
Al	1.082	0.613	0.285	27

TABLE 2

Numerical Results

System	g_c	g_p
γ'	0.170	0.145
Ni	0.173	0.113
Al	0.0810	0.0296

TABLE 3

Values of the Stress-Free Transformation Strain Used in the Critical Particle Size Calculations

System		ε_o	Reference
Matrix	Precipitate		
Ni-Al	γ'	0.0085	31,32
Ni-Ti	γ'	0.0110	33
Al-Li	δ'	-0.0015	36-39

TABLE 4

Critical Particle Sizes (in Å) for the Cube and Plate Shape Transitions

System		Elastic Constants Used	d_c	d_p
Matrix	Precipitate			
Ni-Al	$\gamma'(Ni_3Al)$	$\gamma'(Ni_3Al)$	110	130
Ni-Al	$\gamma'(Ni_3Al)$	Ni	110	170
Ni-Ti	$\gamma'(Ni_3Ti)$	Ni	130	200
Al-Li	$\delta'(Al_3Li)$	Al	3.1μm	8.5μm

TABLE 5

The Anisotropy Factors for the Systems Investigated.

System	Anisotropy Factor, Δ
γ'	-1.395
Ni	-1.212
Al	-0.354

TABLE 6

The Effect of the Anisotropy of Al on the Critical Particle Size (in μm) of δ'

Anisotropy Factor, Δ	d_c
-0.354	3.1
-0.5	2.2
-1.0	1.3
-1.2	1.3

TABLE 7

The Effect of Misfit on the Critical δ' Particle Size (in μm) in Al

ε_o	d_c
0.0015	3.1
0.002	1.7
0.003	0.78
0.004	0.44
0.005	0.28
0.006	0.19
0.007	0.14
0.008	0.11
0.009	0.09

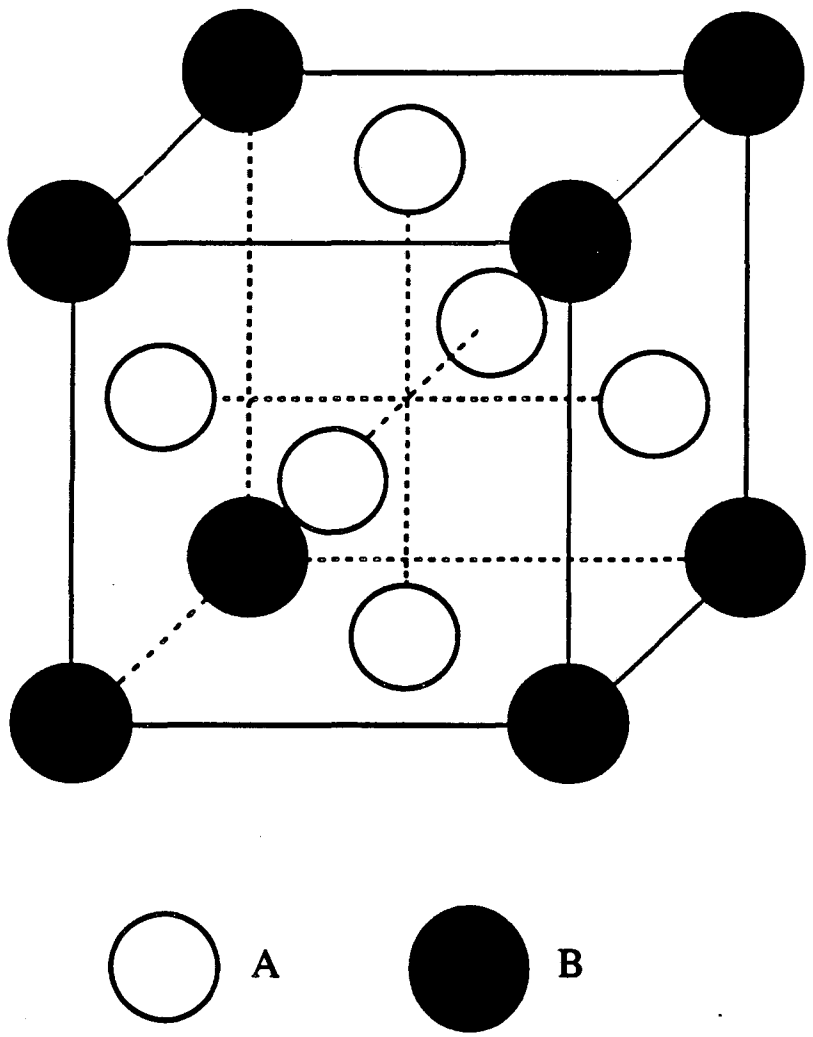

Figure 1. The $L1_2$ crystal structure with the stoichiometric composition A_3B.

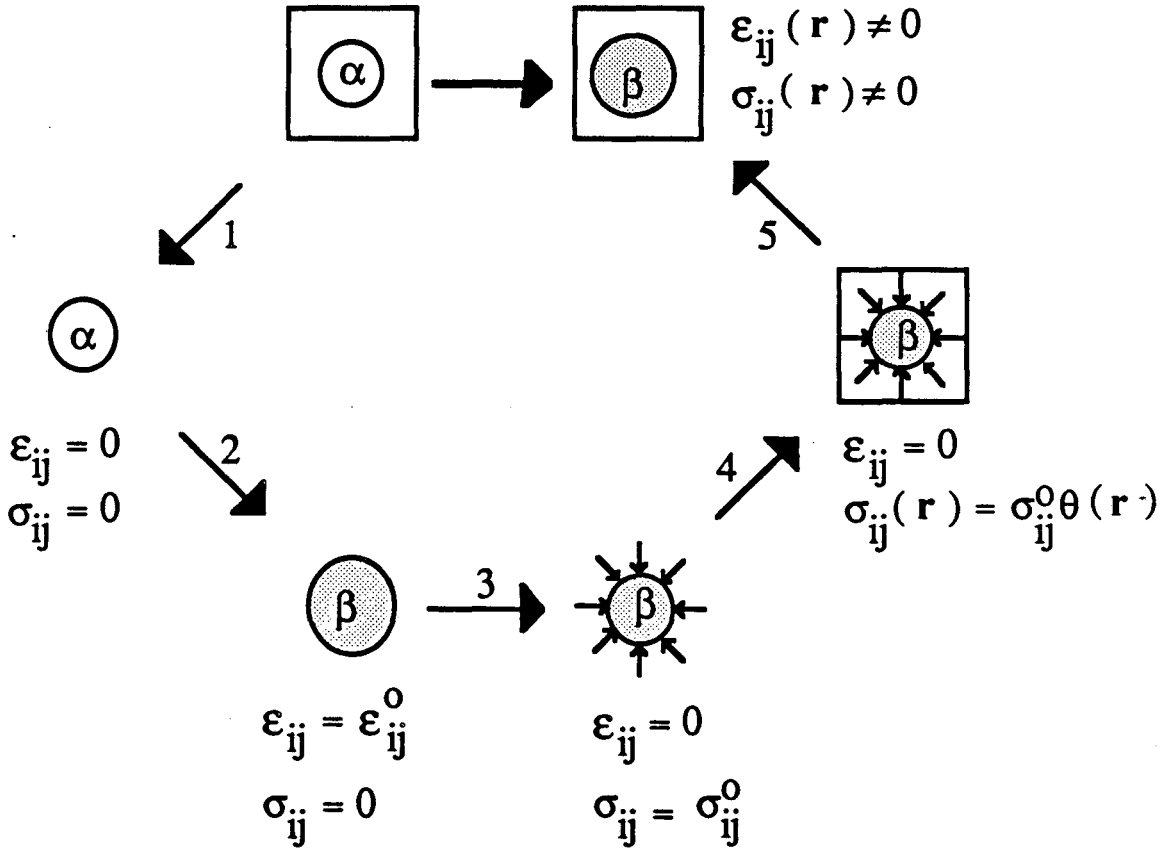

Figure 2. Schematic illustration of the imaginary steps used to model a precipitation reaction. (Eshelby Cycle)

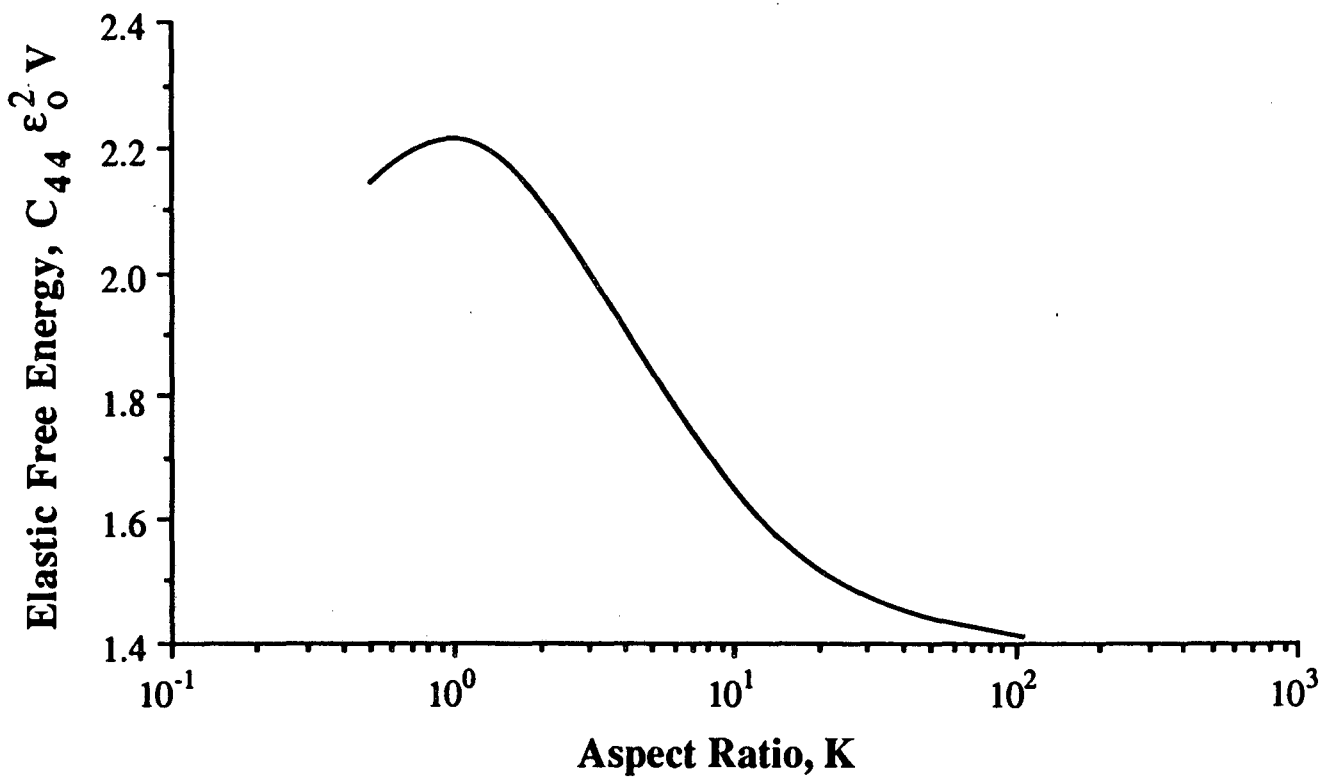

Figure 3. The elastic free energy for an ellipsoidal γ' precipitate as a function of aspect ratio.

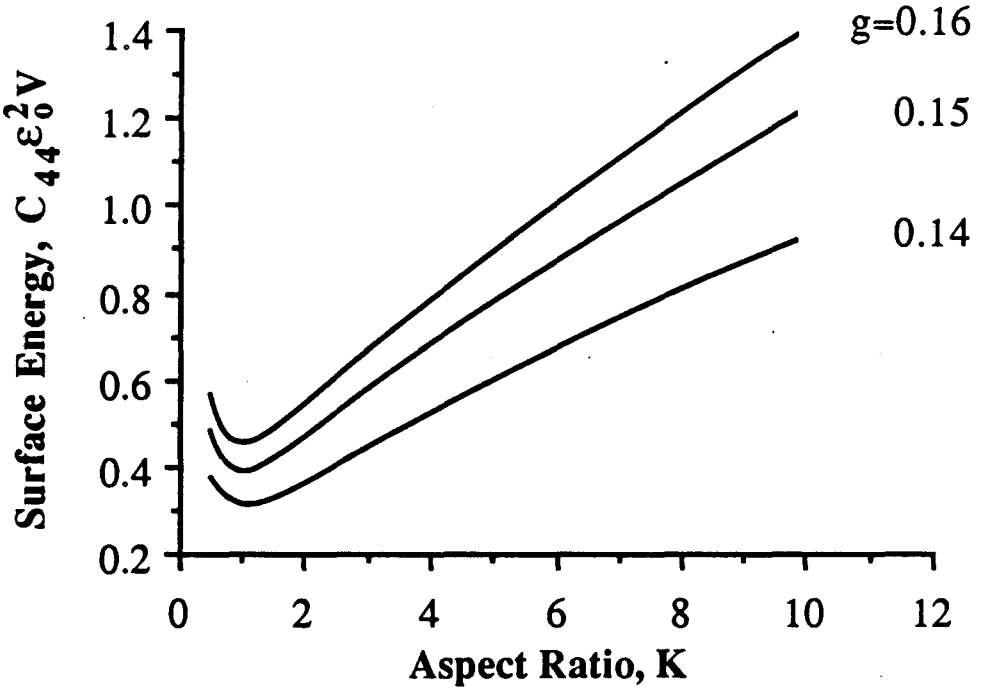

Figure 4. The surface energy for an ellipsoidal precipitate as a function of aspect ratio.

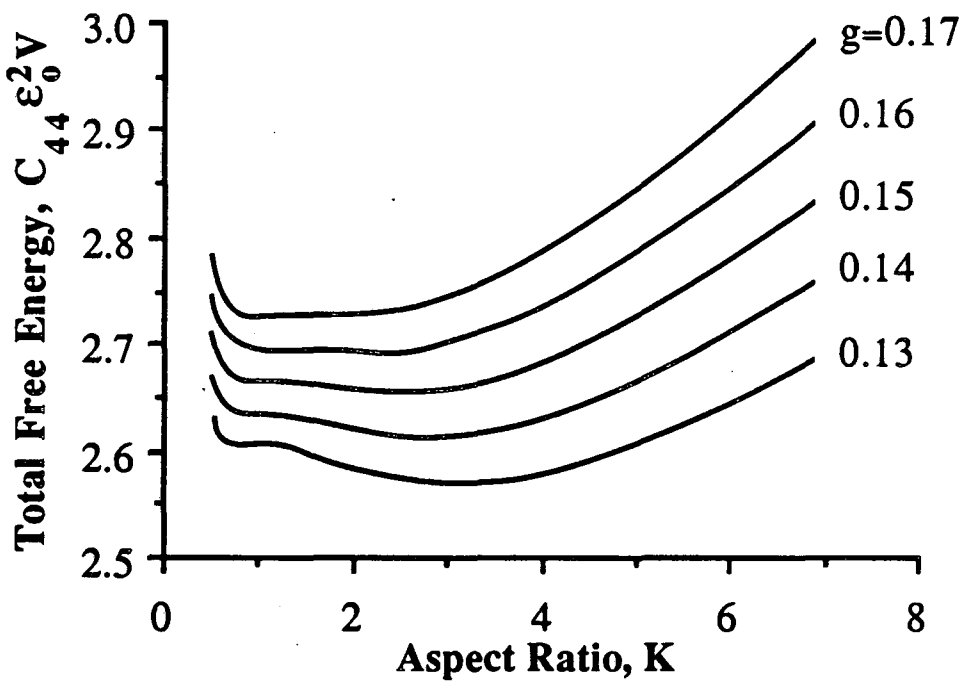

Figure 5. The total free energy of an ellipsoidal γ' precipitate as a function of aspect ratio.

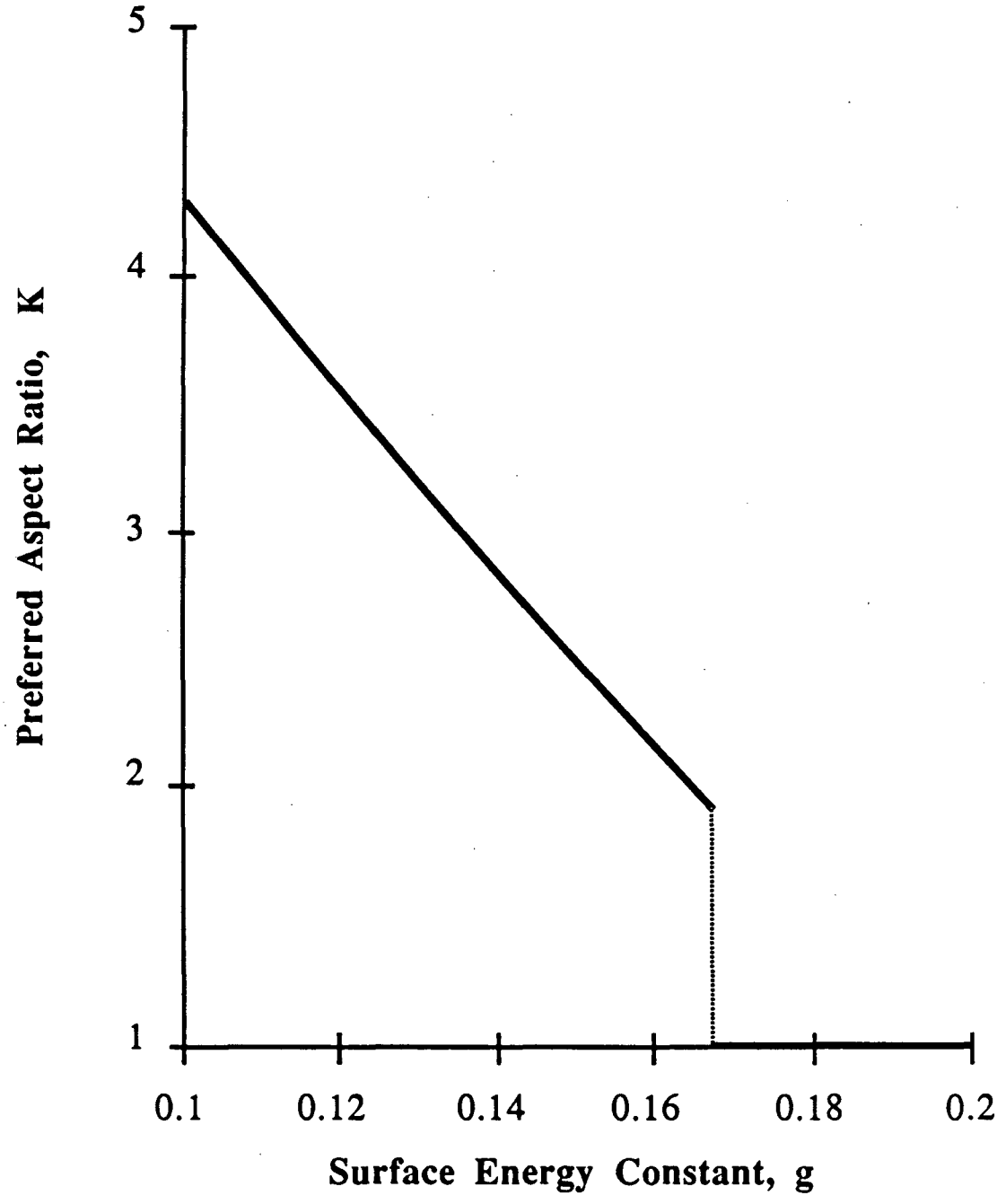

Figure 6. The preferred aspect ratio for an ellipsoidal γ' precipitate as a function of g.

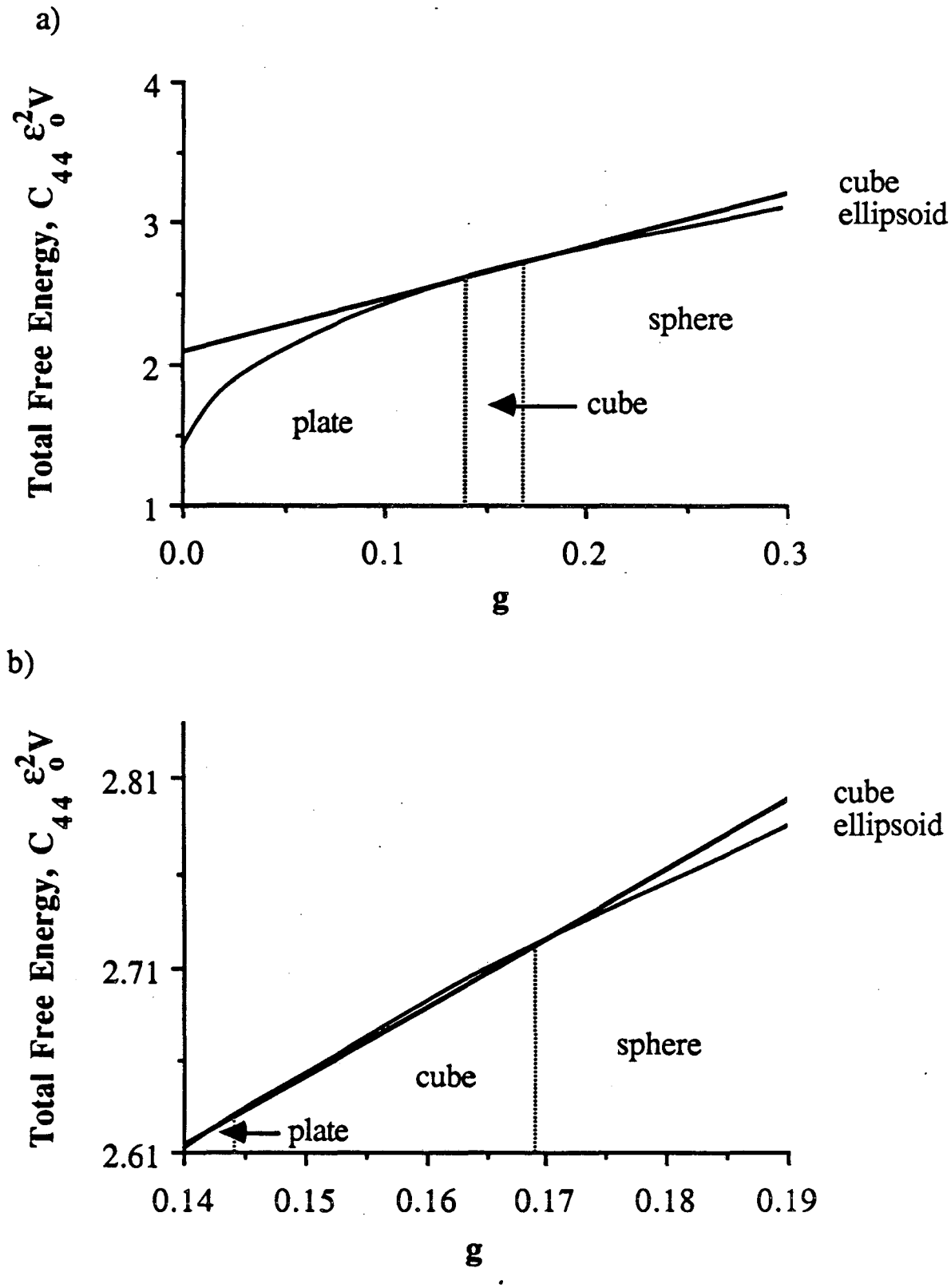

Figure 7. The free energy for an ellipsoidal and a cuboidal γ' precipitate (a) over a wide range of g and (b) for intermediate values of g.

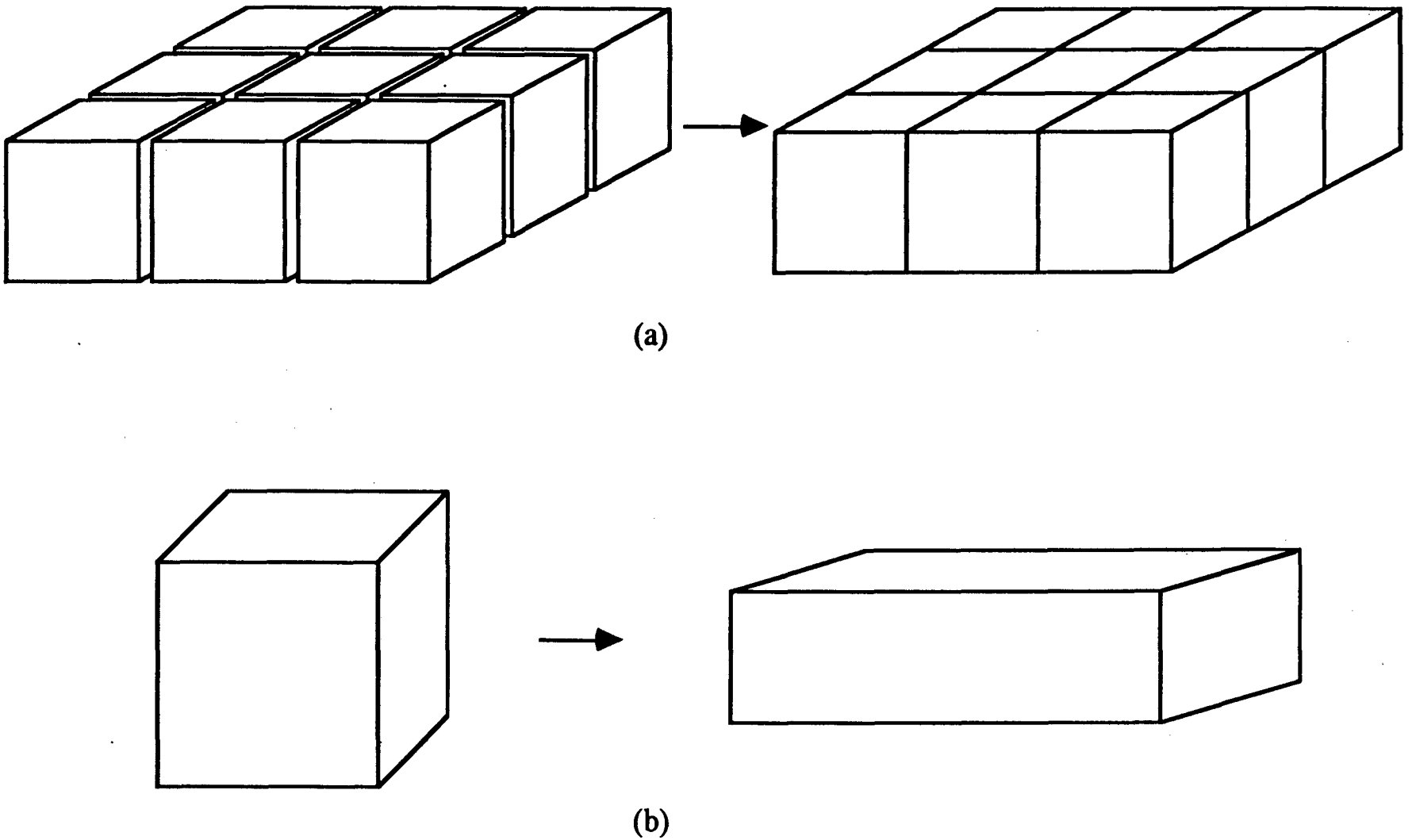

Figure 8. The formation of γ' plates a) as seen in practice and b) by a constant-volume process.

Appendix 1: The Symmetry of the Taylor Expansion Coefficients α_{ij} and λ_{ijkl}

Since the free energy must be invariant to rigid-body rotations (ω_{ij} = a constant), it cannot be a function of $\omega_{ij}(\mathbf{r})$. The free energy, then, depends only on $\varepsilon_{ij}(\mathbf{r})$. The tensors α_{ij} and λ_{ijkl} are Taylor expansion coefficients defined by:

$$\alpha_{ij} = \{\partial\tilde{f}[\boldsymbol{\varepsilon}(\mathbf{r})]/\partial\varepsilon_{ij}(\mathbf{r})\}\,|_{\boldsymbol{\varepsilon}(\mathbf{r})=\mathbf{0}} \tag{A1.1}$$

and

$$\lambda_{ijkl} = \{\partial\tilde{f}[\boldsymbol{\varepsilon}(\mathbf{r})]/\partial\varepsilon_{ij}(\mathbf{r})\varepsilon_{kl}(\mathbf{r})\}\,|_{\boldsymbol{\varepsilon}(\mathbf{r})=\mathbf{0}}. \tag{A1.2}$$

By definition, the infinitesimal strain tensor is symmetric:

$$\begin{aligned}\varepsilon_{ij}(\mathbf{r}) &= (1/2)[u_{i,j} + u_{j,i}] \\ &= (1/2)[u_{j,i} + u_{i,j}] \\ &= \varepsilon_{ji}(\mathbf{r}).\end{aligned} \tag{A1.3}$$

Therefore, reversing the indices for the strain has no effect on the value of equations (A1.1) and (A1.2). The tensor α_{ij} is symmetric,

$$\alpha_{ij} = \alpha_{ji}$$

and (A1.4)

$$\lambda_{ijkl} = \lambda_{jikl} = \lambda_{ijlk}.$$

Since the differentiation in equation (A1.2) may be taken in either order,

$$\lambda_{ijkl} = \lambda_{klij}. \tag{A1.5}$$

Appendix 2: Gauss' Theorem

Gauss' theorem, also known as the divergence theorem, states that a volume integral can be converted into a surface integral by the following relation:

$$\int [f(\mathbf{r})]_{,i} dV = \int f(\mathbf{r}) n_i dS. \tag{A2.1}$$

where n_i is the ith component of the outward normal vector n_i on the surface element dS. The second term in equation (2.1.19) is then equal to the following surface integral:

$$\int [-\sigma^o_{ij}\theta(\mathbf{r})\delta u_i(\mathbf{r}) + \lambda_{ijkl}\delta u_i(\mathbf{r})\varepsilon_{kl}(\mathbf{r})]_{,j} d^3r$$

$$= \int [-\sigma^o_{ij}\theta(\mathbf{r}) + \lambda_{ijkl}\varepsilon_{kl}(\mathbf{r})]\delta u_i(\mathbf{r}) n_j dS. \tag{A2.2}$$

The term in brackets in equation (A2.2) is the local stress on a volume element located at the position **r** in the material. Since the integral above is taken over the surface of the system, it is zero because the stress is zero at the surface.

Appendix 3: The Fourier Transform of the Derivative of a Function

The Fourier transform of the derivative of a function is derived as follows:

$$\begin{aligned} f,_j(\mathbf{r}) &= \partial f(\mathbf{r})/\partial r_j \\ &= (\partial/\partial r_j)[f(\mathbf{k})\exp(i\mathbf{k}\cdot\mathbf{r})d^3k/(2\pi)^3]. \end{aligned} \tag{A3.1}$$

Since the differentiation and the integration are independent of one another, their order may be reversed:

$$\begin{aligned} f,_j(\mathbf{r}) &= \int f(\mathbf{k})(\partial/\partial r_j)[\exp(i\mathbf{k}\cdot\mathbf{r})]d^3k/(2\pi)^3 \\ &= \int [f(\mathbf{k})ik_j]\exp(i\mathbf{k}\cdot\mathbf{r})d^3k/(2\pi)^3. \end{aligned} \tag{A3.2}$$

Since $f,_j(\mathbf{r})$ is a function of **r**, it may be transformed directly as well:

$$f,_j(\mathbf{r}) = \int f,_j(\mathbf{k})\exp(i\mathbf{k}\cdot\mathbf{r})d^3k/(2\pi)^3. \tag{A3.3}$$

For both equations (A3.2) and (A3.3) to hold, it must be true that

$$f,_j(\mathbf{k}) = ik_j f(\mathbf{k}). \tag{A3.4}$$

Using a similar argument,

$$f,_{jk}(\mathbf{k}) = -k_j k_k f(\mathbf{k}). \tag{A3.5}$$

Appendix 4: The Convolution Theorem

The convolution theorem states that

$$\int f(\mathbf{r})g(\mathbf{r})d^3r = \int f(\mathbf{k})g^*(\mathbf{k})d^3k/(2\pi)^3. \tag{A4.1}$$

This is easily shown by taking the Fourier transform of the two functions on the left side of equation (A4.1):

$$\int f(\mathbf{r})g(\mathbf{r})d^3r = \int[\int f(\mathbf{k})e^{i\mathbf{k}\cdot\mathbf{r}}d^3k/(2\pi)^3][\int g(\mathbf{k}')e^{i\mathbf{k}'\cdot\mathbf{r}}d^3k'/(2\pi)^3]d^3r. \tag{A4.2}$$

The right hand side of the above equation is independent of the order of integration. Rearranging then gives

$$\int f(\mathbf{r})g(\mathbf{r})d^3r = \iint f(\mathbf{k})g(\mathbf{k}')d^3kd^3k'/(2\pi)^6\int e^{i(\mathbf{k}+\mathbf{k}')\cdot\mathbf{r}}d^3r$$

$$=\iint[f(\mathbf{k})g(\mathbf{k}')d^3kd^3k'/(2\pi)^6][(2\pi)^3\delta(\mathbf{k}+\mathbf{k}')] \tag{A4.3}$$

$$=\int f(\mathbf{k})g(-\mathbf{k})d^3k/(2\pi)^3$$

$$=\int f(\mathbf{k})g^*(\mathbf{k})d^3k/(2\pi)^3.$$

From equation (2.1.15), then,

$$\int\sigma^o_{ij}\theta(\mathbf{r})\varepsilon_{ij}(\mathbf{r})d^3r = \int\sigma^o_{ij}\theta(\mathbf{k})\varepsilon^*_{ij}(\mathbf{k})d^3k/(2\pi)^3$$

and (A4.4)

$$\int\lambda_{ijkl}\varepsilon_{ij}(\mathbf{r})\varepsilon_{kl}(\mathbf{r})d^3r = \int\lambda_{ijkl}\varepsilon_{ij}(\mathbf{k})\varepsilon^*_{kl}(\mathbf{k})d^3k/(2\pi)^3.$$

Appendix 5: The Shape of a Tetragonal Precipitate in a Cubic Alloy

In the 1960's, a second coherent precipitate which forms in superalloys was discovered. This precipitate is now called γ'' and has the ordered tetragonal DO_{22} crystal structure shown in Figure A5.1. Initially, there was much confusion in the literature mistaking the new tetragonal phase for γ' [A1-A4]. The $\gamma'$and γ'' diffraction patterns are very similar, and it was several years before the existence of γ'' as a separate phase was firmly established. Unlike γ'; γ'', for reasons that will be given in the following, always takes on a plate shape. Therefore, some of the earlier reportings of plate-shaped γ' may actually have been γ''.

The calculations made previously for a cubic precipitate are easily adapted to a tetragonal precipitate by modifying the stress-free transformation strain. Breaking the tetragonal strain up into a pure dilation and an expansion along one axis,

$$\varepsilon^{o}_{ij} = \delta_{ij} + \eta\delta_{33} \quad (\varepsilon_o) \tag{A5.1}$$

where

$$\eta = (\varepsilon_{33}-\varepsilon_o)/\varepsilon_o \tag{A5.2}$$

is the 'tetragonality' of the transformation and ε_o in this case is the amount of dilation (i.e. $\varepsilon_o=\varepsilon_{11}=\varepsilon_{22}$). If equation (2.2.19) is replaced by equation (A5.1), then the elastic free energy may be calculated for an ellipsoid in the same manner as it was previously for a cubic precipitate.

The elastic free energy is plotted against aspect ratio for several values of the tetragonality, η, in Figure A5.2. In this case, a sphere is not an extremum in the elastic free energy. As a result, even if an isotropic surface energy is assumed, a spherical shape can never be stable. The elastic free energy for a tetragonal precipitate drops off to an absolute minimum as the aspect ratio approaches infinity. The preferred shape will therefore be a plate of aspect ratio determined by a balance between the surface and elastic free energies.

REFERENCES

A1. K.M. Chang, Ph.D. Thesis, University of California, Berkeley, CA (1979).

A2. I. Kirman and D.H. Warrington, JISI, 205 (1967), 1264.

A3. P.S. Kotval, Trans. AIME, 242 (1968), 1764.

A4. W.E. Quist, R. Taggart and D.H. Polonis, Met. Trans., 2 (1971), 825.

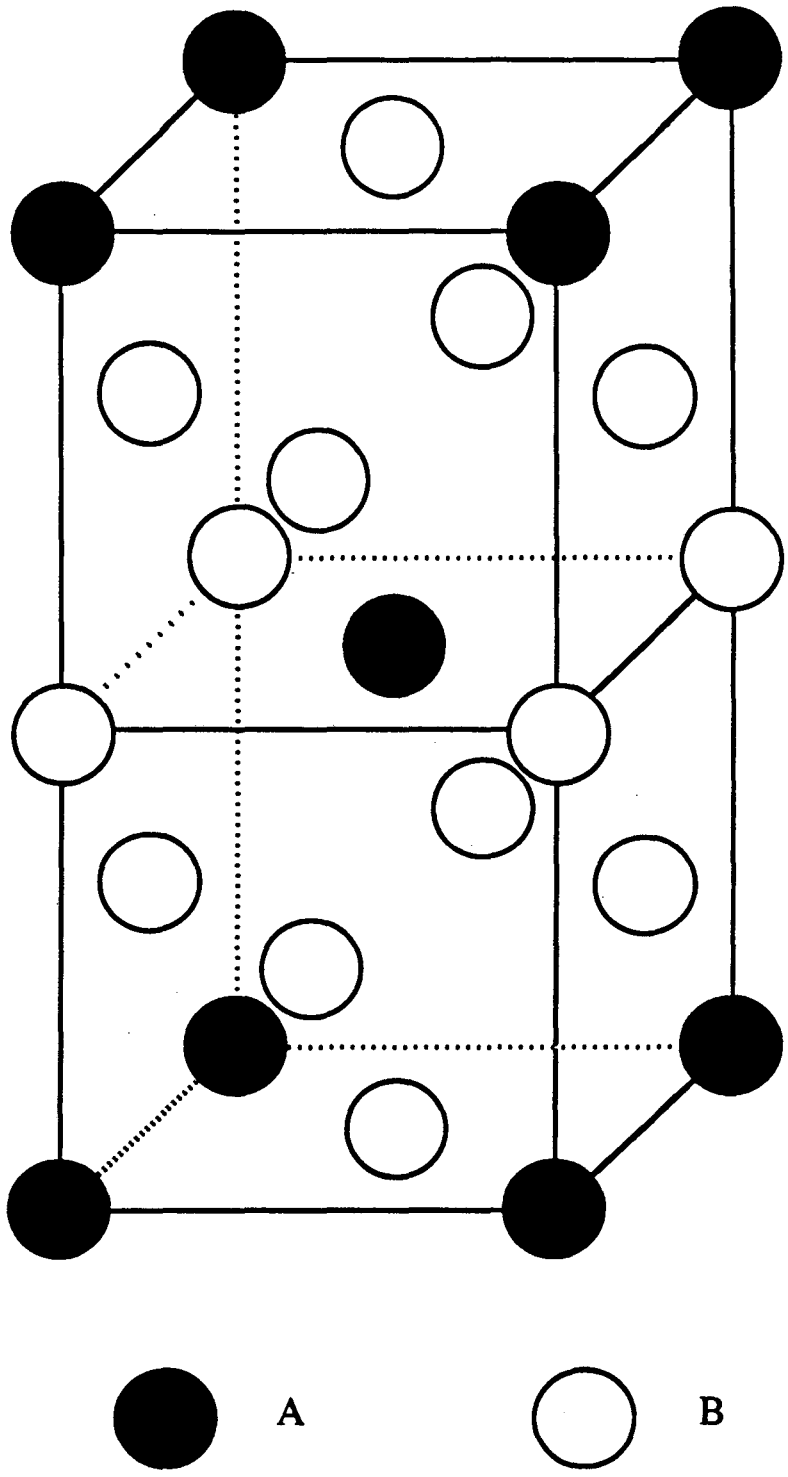

Figure A5.1. The $D0_{22}$ crystal structure with the stoichiometric composition A_3B.

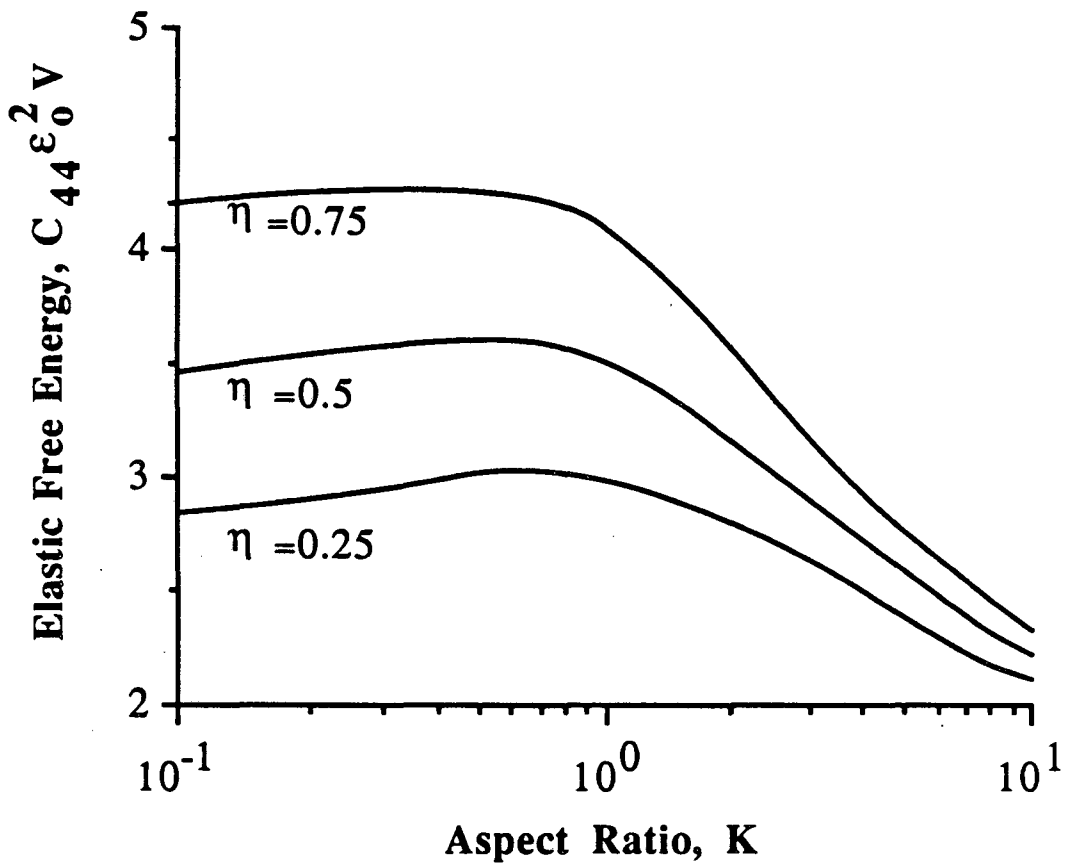

Figure A5.2. The elastic free energy as a function of the aspect ratio of an ellipsoidal precipitate with a tetragonal crystal structure in a cubic matrix.

LAWRENCE BERKELEY LABORATORY
TECHNICAL INFORMATION DEPARTMENT
UNIVERSITY OF CALIFORNIA
BERKELEY, CALIFORNIA 94720